

Supporting Information

Tumor-Targeting [2]catenane-Based Grid-Patterned Periodic DNA Monolayer Array for *in Vivo* Theranostic Application

Yan-Ru Chen,[‡] Shujuan Sun,[‡] Hongwei Yin, Weijun Wang, Ran Liu, Huo Xu, Ya Yang and Zai-Sheng Wu*

Cancer Metastasis Alert and Prevention Center, Fujian Provincial Key Laboratory of Cancer Metastasis Chemoprevention and Chemotherapy, State Key Laboratory of Photocatalysis on Energy and Environment, College of Chemistry, Fuzhou University, Fuzhou, 305108, China

E-mail: wuzhaisheng@163.com

Table of Contents

1. Experimental Procedures

SA.1 Stability analysis of DNA assemblies

SA.2 Comparative analysis of payload capability of [2]GDA, IPSa, IPSb, PSa and PSb

SA.3 Flow cytometry analysis

SA.4 Confocal fluorescence microscopy imaging

SA.5 MTT assay

SA.6 *In vivo* experiments

SA.7 Experimental procedure for Figure 1 in the text

2. Supporting Tables and Figures

SB.1 Supporting Tables

SB.2 Supporting Figures

3. Supporting References

1. Experimental Procedures

SA.1 Stability analysis of DNA assemblies

A 0.5- μ L aliquot of DNase I and 2.8 μ L of 10 \times DNase I buffer were added into 25 μ L of [2]GDA-DF (assembled in the section of “Preparation of catenane-based grid-patterned DNA arrays (GDA)”) or [4]GDA (assembled as shown in **Figure S20**), followed by incubation at 37 $^{\circ}$ C for the different time periods (0–24 h). Finally, heat inactivation of DNase I at 75 $^{\circ}$ C for 20 min was performed. The final concentration of DNase I was 3 U/mL.

The resistance of [2]GDA and [4]GDA to FBS or Exo I was explored according to the same procedure as that adopted above, but 0.5 μ L of ddH₂O and 2.8 μ L of FBS (or 0.5 μ L of Exo I and 2.8 μ L of 10 \times Exo I buffer) was used instead of 0.5 μ L of DNase I and 2.8 μ L of 10 \times DNase I buffer, respectively. The final concentrations of FBS and Exo I were 10% FBS and 0.4 U/ μ L, respectively. All samples were analyzed by 8% nPAGE, and quantitative analysis of gel bands was performed by employing Image J.

The fluorescence resonance energy transfer (FRET) measurement was also conducted to confirm the structural resistance of [2]GDA to enzymatic degradation. The degradation experiments were described as described above. After incubating with specific concentration of enzyme or FBS for given time periods, the resulting sample (about 28 μ L) was diluted with 1 \times T4 DNA Ligase buffer to 200 μ L and mixed well. All the fluorescence measurements were carried out on a Hitachi F-7000 fluorescence spectrometer (Hitachi, Ltd., Japan) with a Xenon lamp as the excitation source. The excitation wavelength was fixed at 525 nm (donor Cy3) and the emission range was collected from 545 nm to 750 nm, where the fluorescence intensity (FI) at 672 nm was used to evaluate the FRET efficiency. Specifically, the FRET efficiency was calculated according to the equation: $(FI_t - 13.8)/(FI_0 - 13.8)$. FI_t and FI_0 represent the Cy5 FI at 672 nm from [2]GDA after and before degradation treatment for a given time period, respectively. The value of 13.8 denotes the Cy5 FI at 672 nm measured from the mixture of PSa-2-Cy3 and RS-Cy5 where two strands remain well separate from each other (see the details in **Figure S9** and **Figure S10**), which was considered to be equivalent to the complete degradation of [2]GDA-DF. In addition, the fluorescence pictures of samples were taken in 96-well plate by Amersham Typhoon Trio Variable equipment Mode Imager (G.E. Healthcare, USA) with Cy3 laser channel.

SA.2 Comparative analysis of payload capability of [2]GDA, IPSa, IPSb, PSa and PSb

[2]GDA, IPSa, IPSb, PSa and PSb were pre-assembled according to the section of “Preparation of catenane-based grid-patterned DNA arrays (GDA)”. Then, different contents of DNA assemblies in 1 \times T4 DNA Ligase buffer were separately added to DOX (10 μ L, 40 μ M), and the resulting solutions were incubated for 4 h at 37 $^{\circ}$ C. Finally, additional 1 \times T4 DNA Ligase buffer was added to increase the final volume to 200 μ L. The fluorescence measurement was performed on Hitachi F-7000 (Hitachi Ltd., Japan) with a Xenon lamp as the excitation source, and the excitation wavelength was set at 488 nm.

SA.3 Flow cytometry analysis

Cy5-labeled [2]GDA was assembled from PSa-2 and PSb-2-Cy5 to evaluate the cellular uptake efficiency of [2]GDA. HeLa cells were seeded on a six-well culture plate and cultured in DMEM medium supplemented with 10% fetal bovine serum, 100 μ g/mL streptomycin and 100 U/mL penicillin for 24 h in a humidified atmosphere of 5% CO₂ at 37 $^{\circ}$ C. Subsequently, the resulting HeLa cells (1×10^5 cells) were washed twice with 0.5 mL of SCJ and then incubated in fresh DMEM medium (800 μ L) in the presence of [2]GDA-Cy5 or IPSb-2-Cy5, in each of which the PSb-2-Cy5 concentration was 50 nM. After the incubation of 4 h, the HeLa cells were washed twice with 0.5 mL of SCJ again and resuspended in 1 mL of SCJ. Flow cytometric analysis was performed on a CytoFLEX flow cytometer (Beckman Coulter Biotechnology Co., Ltd, USA).

Moreover, the cell permeability of [2]GDA was studied by comparing with commercial transfection reagent. The Lipofectamine® 3000 Transfection Reagent Kit was used because it was often employed to transport nucleic acids into diseased cells due to its high transfection efficiency,^[S1] and the transfection of DNA nanostructures was conducted according to the manufacturer's protocol. Specifically, the transfection process was described as below. **Solution A:** 3.75 μL of Lipofectamine® 3000 Transfection Reagent (Lip3000) was added into 121.25 μL of Opti-MEM (Gibco) and mixed well at room temperature. **Solution B:** 70 μL of Opti-MEM was mixed with 50 μL of pre-prepared [2]GDA-DF, followed by addition of 5 μL of P3000™ Reagent. [2]GDA-DF, [2]GDA doubly modified with Cy3 and Cy5, was pre-assembled from PSa-2-Cy3 and PSb-2-Cy5 according to the same procedure as [2]GDA. Subsequently, Solution B was added into Solution A drop by drop with stirring and kept at room temperature for 15 min. After diluting with 550 μL of Opti-MEM, the resulting solution was called [2]GDA-Cy5/transfection solution (800 μL), in which HeLa cells were incubated for 4 h. The resulting cells were washed twice with 0.5 mL of SCJ and resuspended in 1 mL of SCJ. Flow cytometric analysis was performed on a CytoFLEX flow cytometer (Beckman Coulter Biotechnology Co., Ltd, USA).

Besides, for the cell apoptosis analysis, the HeLa cells were immersed in fresh DMEM medium (800 μL) containing a given concentration of [2]GDA (10 nM, 40 nM, 80 nM, 150 nM or 200 nM). After incubating at room temperature for 24 h, the resulting cells were treated by Annexin V-TITC&PI cell death detection kit according to the instruction. Flow cytometric analysis was performed on a CytoFLEX flow cytometer (Beckman Coulter Biotechnology Co., Ltd, USA).

SA.4 Confocal fluorescence microscopy imaging

HeLa cells were cultured on a twelve-well culture plate for 24 h and grown to 70~80% confluency. Subsequently, to evaluate the cellular uptake efficiency in a comparative format, the culture medium was substituted by the mixture (400 μL) of DMEM medium and Cy5-GDA ([2]GDA or [4]GDA), IPSb-2-Cy5 or PSb-2-Cy5 (each containing 50 nM Cy5-labeled component). After incubated for given time periods and washed with SCJ solution, the cell nuclei were stained with Hoechst 33342 (10 $\mu\text{g}/\text{mL}$) for 15 min at 37 °C. After washing with SCJ solution, the confocal fluorescence microscopic imaging of cells was conducted on a confocal laser fluorescence microscopy (Leica TCS SP8). Fluorescence quantitative analysis of cell images was performed by employing Image J.

In order to investigate the cellular stability of [2]GDA by measuring FRET change, [2]GDA-DF was incubation with HeLa cells for defined time periods, while PSa-2-Cy3 was employed as the control. Because PSa-2-Cy3 cannot actively enter the cells and all the experiments should be performed under identical conditions, the commercial transfection reagent (Lipofectamine® 3000 Transfection Reagent Kit) was used in this section and the manufacturer's transfection protocol was adopted. The transfection process was briefly described as below. **Solution A:** 1.5 μL of Lip3000 was added into 48.5 μL of Opti-MEM (Gibco) and mixed well at room temperature. **Solution B:** 23 μL of Opti-MEM was mixed with 25 μL of [2]GDA-DF, followed by adding 2 μL of P3000™ Reagent and mixing well. Subsequently, Solution B was added into Solution A drop by drop with stirring and kept at room temperature for 15 min. After diluting with 300 μL of Opti-MEM, the resulting solution (400 μL) was called [2]GDA-DF/transfection solution. Afterwards, HeLa cells (1×10^5 cells) were incubated in [2]GDA-DF/transfection solution for 4 h, followed by washing with SCJ solution. The fresh DMEM medium supplemented with 10% FBS and 1% penicillin-streptomycin was added and incubated for different time periods (0 h, 5 h and 10 h). After washing with SCJ solution again, the cell nucleus was stained with Hoechst 33342 (10 $\mu\text{g}/\text{mL}$) for 15 min. The confocal fluorescence microscopic imaging of the cells was conducted on a

confocal laser fluorescence microscopy (Leica TCS SP8). PSa-2-Cy3 was transfected by Lip3000 into cells according to the same procedure.

The cytotoxicity of [2]GDA-DOX was inspected by counting the cell density through confocal fluorescence microscopy imaging. [2]GDA-DOX solution containing 10 μ M DOX was used to treat HeLa cells by incubation for 4 h, followed by washing with SCJ solution. The fresh DMEM medium supplemented with 10% FBS and 1% penicillin-streptomycin was added and incubated for another 20 h. After washing with SCJ solution again, the cell nucleus was stained with Hoechst 33342 (10 μ g/mL) for 15 min. As the controls, HeLa cells were separately treated with free DOX, IPSa-DOX, IPSb-DOX, PSa-DOX and PSb-DOX according to the same procedure at the equivalent concentration of DOX. The confocal fluorescence microscopy imaging was conducted with a confocal laser fluorescence microscopy (Leica TCS SP8). Moreover, the cytotoxicity of these formulations to cells was also evaluated by MTT assay (seen below).

SA.5 MTT assay

The biocompatibility of [2]GDA was evaluated through cellular cytotoxicity study by MTT assay. HeLa cells were seeded on 96-well culture plate and grown to 70~80% confluency for 24 h. Afterwards, the cells were treated with different concentrations of [2]GDA in 100 μ L of DMEM medium without FBS for 4 h. After substituting the supernatant medium with 100 μ L of 10% FBS-contained DMEM medium, the incubation was allowed to proceed for 20 h. Then, the resulting cells were washed with SCJ solution and incubated with 150 μ L of MTT reagent at 37 $^{\circ}$ C for 4 h. After removing MTT reagent and washing with SCJ solution again, 100 μ L of DMSO was added into each well and incubated for 10 min with shaking at 600 rpm. Finally, the absorbance at 450 nm was measured on multimode plate reader (Tecan Infinite M200 PRO, Switzerland). In addition, the cellular cytotoxicity of [2]GDA-DOX was evaluated according to the same processes.

SA.6 *In vivo* experiments

For *in vivo* confocal fluorescence imaging, the male BALB/c nude mice (20–25 g) received a subcutaneous injection of 1×10^7 HeLa cells in the right axilla. The tumor-bearing mice were fed normally for 25–30 days until the tumors grew to about 700 mm^3 in size. After anesthetized with 1.0-1.5% isoflurane, tumor-bearing mice were injected with Cy5-labeled [2]GDA (100 μ L, 1 mM) intravenously via a single tail vein. At given time points, the fluorescence images of live mice were captured by IVIS-spectrum imaging system (Perkin-Elmer, USA). The normal mice administrated with Cy5-labeled [2]GDA under identical conditions were imaged to offer the controls.

Besides *in vivo* fluorescence imaging, more mice were systemically administered with Cy5-labeled [2]GDA according to the same procedure and then the organs were harvested at different time points post-injection for the *ex vivo* organ imaging to offer more information about the *in vivo* biodistribution and decay kinetics. The sequence-scrambled rPSa-2-Cy5 without obvious secondary structure was employed as control.

In order to investigate the inhibitory effect of [2]GDA-DOX on tumor growth, tumor-bearing nude mouse model was established according to the above processes. When tumor volume reached about 300 mm^3 , tumor-bearing nude mice were randomly divided into five groups and five mice were involved in each group. They were intravenously injected with saline, free DOX, IPSa-DOX, IPSb-DOX or [2]GDA-DOX (DOX, 500 μ g/kg) every 3 days for 18 days. The tumor size was estimated by a digital caliper, while the body weight was determined by an electronic balance before each administration. The tumor volume was calculated by the formula $(a^2b)/2$, where a and b are the width and length of tumor, respectively. After the last treatment, the tumors and major organs (heart, liver, spleen, lung

and kidney) were harvested for histological analysis according to the literature method.^[S2] All animal experiments were approved by the Institutional Animal Care and Use Committee (IACUC) of Fuzhou University (approval number: 784 SYXK-2019-0007).

SA.7 Experimental procedure for Figure 1 in the text

The Figure 1C: For sample ①, 1.6 μM PSa-2 in 1 \times T4 DNA Ligase buffer (12.5 μL) was annealed at 90 $^{\circ}\text{C}$ for 5 min and then allowed to cool down to room temperature slowly. Afterwards, 12.5 μL of 1 \times T4 DNA Ligase buffer was added to form a final volume of 25 μL . For sample ②, the experimental procedure was the same as that adopted for preparing sample ①, but PSb-2 was used instead of PSa-2. The procedures used for the preparation of sample ③ and sample ④ are shown in the section of “Preparation of catenane-based grid-patterned DNA arrays (GDA)” .

2. Supporting Tables and Figures

SB.1 Supporting Tables

Table S1. Sequences of oligonucleotides designed in this work

Note	Sequence (5→3)
[2]GDA	Phosphorylated strand a1 (PSa-1) P- CTTACCTGATAGCGCGCGCT T TAGAACGAGTCATATCACAC GCCCCGGGGC ACTACTAAC
	Phosphorylated strand b1 (PSb-1) p- ACTCGTTCTAAGCGCGCGCT ATCAGGTAAGGTTAGTAGTG CCCCGGGGC GTGTGATATG
	Strand a2 (Sa-2) GCTTACCTGATAGCGCGCGCT TTAGAACGAGTCATATCAC ACAAGCCCCGGGGG ACTACTAACCT
	Phosphorylated strand a2 (PSa-2) p- GCTTACCTGATAGCGCGCGCT TTAGAACGAGTCATATC ACACAA GCCCCGGGGG ACTACTAACCT
	Phosphorylated strand a2-Cy3 (PSa-2-Cy3) p- GCTTACCTGATAGCGCGCGCT TTAGAACGAGTCATATC ACACAA /icy3dt/ GCCCCGGGGG ACTACTAACCT
	Strand b2 (Sb-2) ACTCGTTCTAAAGCGCGCGCT ATCAGGTAAGCAGGTTAGT AGTGCCCCGGGGG TTGTGTGATATG
	Phosphorylated strand b2 (PSb-2) p- ACTCGTTCTAAAGCGCGCGCT ATCAGGTAAGCAGGTTA GTAGTGCCCCGGGGG TTGTGTGATATG
	Phosphorylated strand b2-Cy5 (PSb-2-Cy5) p- ACTCGTTCTAAAGCGCGCGCT ATCAGGTAAGCAGGTTA GTAGTGCCCCGGGGG /icy5dt/ TTGTGTGATATG
	Phosphorylated strand a3 (PSa-3) p- GGCTTACCTGATAGCGCGCGCGCT TTAGAACGAGTCGC ATATCACACA GCCCCGGGGG ACTACTAACCTA
	Phosphorylated strand b3 (PSb-3) p- GACTCGTTCTAAAGCGCGCGCT ATCAGGTAAGCCTA GGTTAGTAGTGCCCCGGGGG TTGTGTGATATGC
[4]GDA	Phosphorylated strand a4-1 (PSa-4-1) p- CTTACCTGATTTGCTGCTACGGACG TTAGAACGAGTCATA TCACACTCTCTGTCACATCG TTACTACTAAC
	Phosphorylated strand a4-1-Cy5 (PSa-4-1-Cy5) p- CTTACCTGAT /icy5dt/ TTGCTGCTACGGACG TTAGAACGAGTCATACACTCTCTGTCACATCG TTACTACTAAC
	Phosphorylated strand a4-2 (PSa-4-2) p- CTTACCTGATTTGCTGCTACGGACG TTAGAACGAGTCATA TCACACTCGATGTGACAGAG TTACTACTAAC
	Phosphorylated strand b4-1 (PSb-4-1) p- ACTCGTTCTATTGCTCGAAAGTTG TATCAGGTAAGGGTT AGTAGTTCTCTGCTCTAGG TTGTGTGATATG
	Phosphorylated strand b4-2 (PSb-4-2) p- ACTCGTTCTATTGCTCGAAAGTTG TATCAGGTAAGGGTT AGTAGTTCTTAGAGACAGAG TTGTGTGATATG
Random strand	Random Phosphorylated strand a-2 (rPSa-2) p-GCTTCCCACCGTGGATAGCCGCTTAGAGCTACGAGTCATA TCACAGCGCAACGGGCACTACTGCAACCT
	Random Phosphorylated strand a-2-Cy5 (rPSa-2-Cy5) p-GCTTCCCACCGTGGATAGCCGCTTAGAGCTACGAGTCATA TCACAGCGCAACGGGCACTACTGCAACCT-Cy5
	Random Phosphorylated strand b-2 (rPSb-2) p-ACTCAGCCTGTTGGCAAAGCATGTCAGGTACGCAGCAGGT TCGTAGTCGGAGTCGTTGTGTGAGCCCTG
	Random strand-Cy5 (RS-Cy5) GTGAACCGTGACCAGTACGTT/icy5dt/TTCCGATTGGCA GTAAGCGTTTTTTAGCACATGGAATGTTCTAGGCCTATACGAGC GATG

^aFor DNA components for the assembly of [2]GDA, the domains with the gray background and the underlined domains in the phosphorylated- and unphosphorylated Sa strands, including PSa-1, Sa-2, PSa-2, PSa-3 and their fluorescently-modified counterparts, are designed to be complementary to the corresponding domains of Sb strands (PSb-1, Sb-2, PSb-2, PSb-3 and their fluorescently-modified counterparts), while the red and green domains indicate the fragments with different palindromic sequences. Thus, the intermolecular hybridization can occur between Sa strands or Sb strands. More details on the interaction between DNA components are described in **Figure 1**. Different from the components of [2]GDA, four different DNA strands without palindromic sequences (PSa-4-1, PSa-4-2, PSb-4-1 and PSb-4-2) are required for the assembly of [4]GDA that is based on the common Watson–Crick base pairing. The red and green domains of PSa-4-1 are complementary to the corresponding domains indicated in PSa-4-2. Similarly, the red and green fragments of PSb-4-1 can hybridize to the corresponding fragments of PSb-4-2. The underlined fragment and purple domains in PSa-4-1 and PS-4a-2 are able to hybridize with the corresponding domains in PSb-4-1 and PSb-4-2, respectively. More details on the hybridization among DNA components of [4]GDA are illustrated in **Figure S20**. rPSa-2 and rPSb-2 are two strands containing the same number of four bases (A, T, G and C) as PSa-2 and PSb-2, respectively, but the bases are arranged in a random manner. Thus, they don't hybridize each other. The sequence-scrambled RS-Cy5 was designed to be unable to hybridize with PSa-2-Cy3, and the mixture of RS-Cy5 and PSa-2-Cy3 was used to evaluate the spurious state of fluorescently dual-labeled [2]GDA completely digested by nucleases. More details are presented in in **Figure S9**.

Table S2. Comparison of enzymatic degradation resistance between [2]GDA and previous DNA nanostructures.

Number	Category	Test conditions	Anti-degradation performance	Ref.
1	DTP-based logic gate nanomachine	10% FBS	> 6 h	[S3]
2	Framework nucleic acid (FNA) nanodevice (DTP-3WBE)	Intracellular	> 8 h	[S4]
3	A bioconjugate between duplex oligodeoxynucleotides and a dendrimer (dODNs-DEN)	Turbo DNase (2 U/ μ L)	About 10 h	[S5]
4	DNA tetrahedral nanostructure (single-armed TDNs, sa-TDN)	80% mice serum	12 h	[S6]
5	A catenane-based grid-patterned periodic DNA monolayer array named [2]GDA	10% FBS	> 24 h	This study
		Intracellular	> 10 h	
		DNase I (3 U/mL)	> 24 h	
		Exo I (0.4 U/ μ L)	> 2 h	
		<i>in vivo</i> (mouse)	> 340 min	

SB.2 Supporting Figures

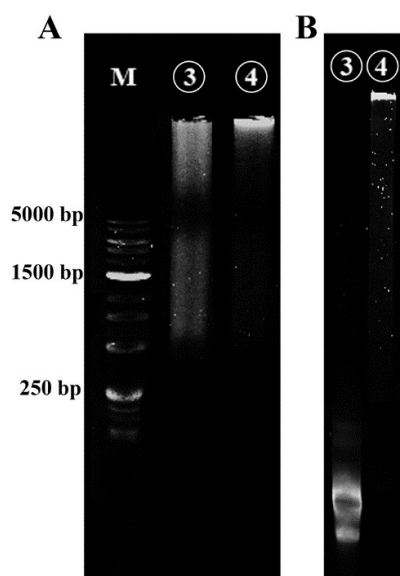


Figure S1. Agarose gel electrophoresis (AGE, 2%) (A) and denaturing polyacrylamide gel electrophoresis (dPAGE, 10%) (B) based analyses of DNA assembled products: Lane ③, nc-[2]GDA; Lane ④, [2]GDA. The DNA products were assembled as depicted in the section of “Preparation of catenane-based grid-patterned DNA arrays (GDA)”, while the gel electrophoresis analyses were carried out as shown in the section of “Gel electrophoresis”.

Discussion:

As shown in the AGE images (**Figure S1A**), two very wide bands are observed in Lane ③, implying the size polydispersity of nc-[2]GDA. This is closely associated with the structural complexity originating from the nicks existing in nc-[2]GDA. In contrast, there is only one main band in the large molecular weight range in Lane ④, suggesting a high degree of monodispersity of [2]GDA. To explore further the dependence of [2]GDA structure on the ligation-based catenation, the dPAGE analysis was conducted. As shown in **Figure S1B**, most of the assembled products (more than 90%) in Lane ④ do not exhibit an obvious gel electrophoretic mobility shift, while all the nc-[2]GDAs in Lane ③ are broken apart into small fragments, demonstrating the fragility of the nick-contained structure.^[S7] These experimental results demonstrate that the ligation-based cyclization of DNA components is of great importance for the assembly of expected [2]GDA.

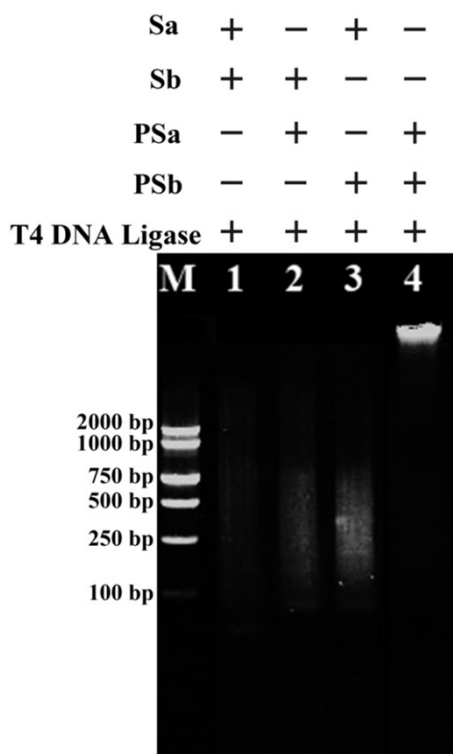


Figure S2. Effect of phosphorylation of DNA components on the assembly of [2]GDA evaluated by agarose gel electrophoresis (AGE) analysis: Lane 1, Sa + Sb + T4 DNA ligase; Lane 2, PSa + Sb + T4 DNA ligase; Lane 3, Sa + PSb + T4 DNA ligase; Lane 4, PSa + PSb + T4 DNA ligase.

Experimental information:

The samples were prepared according to the procedure described in the section of “Preparation of catenane-based grid-patterned DNA arrays (GDA)”, but one or two nonphosphorylated component strands were instead used in Lanes 1 to 3. For example, for Lane 1, Sa-2 and Sb-2 were used instead of PSa-2 and PSb-2, respectively.

Discussion:

For Lane 1 to Lane 3, the ligation-based cyclization of one or two types of DNA components cannot occur because Sa-2 and/or Sb-2 were not phosphorylated. Thus, the perfect catenation between two types of DNA components is unable to be formed. As a result, the DNA components can separate from each other under unfavorable conditions to a greater or lesser extent. Specifically, for Lane 1, both Sa-2 and Sb-2 are completely separate from each other even if the mixture was treated with ligase. Thus, no any fluorescence signal is detected. Only linear catenated IPSa-2 and IPSb-2 were formed in Samples 2 and 3, respectively. Thus, it is reasonable that DNA assembly band with low fluorescence intensity is observed in Lane 2 and Lane 3. This situation contrasts with that for [2]GDA.

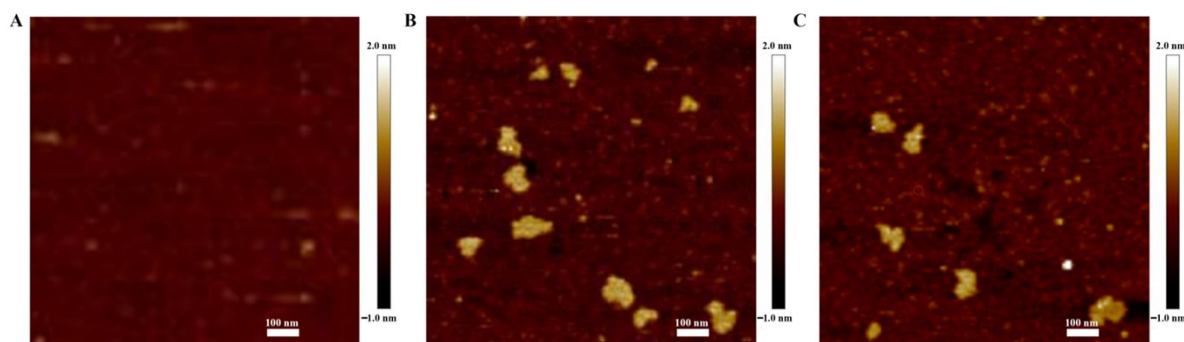


Figure S3. AFM images of annealed PSa-4-1 without palindromic sequences (A), annealed PSa with palindromic sequences (i.e., lPSa) (B) and annealed PSb with palindromic sequences (i.e., lPSb) (C).

Experimental procedure:

For the AFM analysis of **Figure S3A**, 800 nM PSa-4-1 in 1×T4 DNA Ligase buffer was annealed at 90 °C 5 min and then cooled down to room temperature slowly. Similarly, for **Figure S3B** or **Figure S3C**, PSa-2 solution or PSb-2 solution was annealed under identical conditions. AFM imaging was performed as described in the section of “AFM imaging”.

Discussion:

Almost nothing appears in **Figure S3A**, but a few nanosheets with the height of about 1.5 nm and the width of tens of nanometers are observed in **Figure S3B** and **Figure S3C**. This is because the intermolecular interaction cannot occur between PSa-4-1 species and thereby there is no obvious assembled nanostructure within PSa-4-1. Thus, it is still a single-stranded DNA even subjected to the annealing treatment. By AFM, it is difficult to visualize the morphology of PSa-4-1. Unlike PSa-4-1, one PSa-2 or PSb-2 has two different palindromic domains and thus the intermolecular hybridization occurs, easily assembling into the nanoscale products especially after annealing treatment. The as-assembled products are able to be observed by AFM.

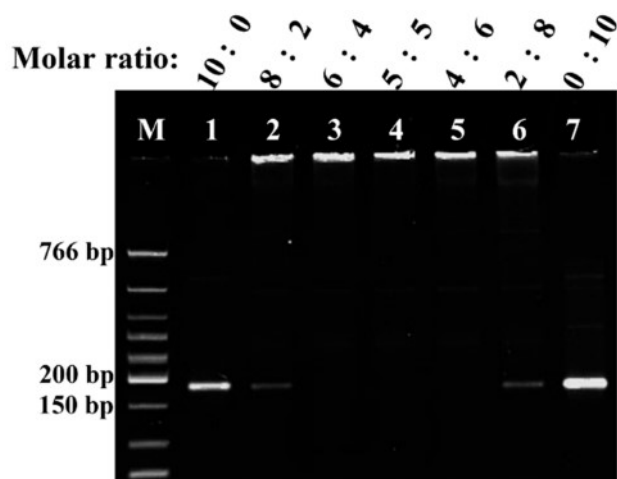


Figure S4. The dependence of [2]GDA assembly efficiency on the molar ratio of two components. nPAGE analysis of [2]GDA assembled at the different molar ratios of PSa/PSb: Lane 1, 10:0; Lane 2, 8:2; Lane 3, 6:4; Lane 4, 5:5, Lane 5, 4:6, Lane 6, 2:8, Lane 7, 0:10. There is no residual DNA component band (PSa or PSb) in Lane 3, Lane 4 and Lane 5, proving that almost all the PSa and PSb are assembled into [2]GDA when the molar ratio of PSa/PSb ranges from 6:4 to 4:6.

Experimental information:

The samples were prepared according to the procedure described in the section of “Preparation of catenane-based grid-patterned DNA arrays (GDA)”. While the total concentration of two DNA components remained constant, the PSa-2/PSb-2 ratio was changed. Namely, for samples 1 to 7, the concentration of DNA components is described below: 1600 nM PSa-2 and 0 nM PSb-2 (10:0), 1280 nM PSa-2 and 320 nM PSb-2 (8:2), 960 nM PSa-2 and 640 nM PSb-2 (6:4), 800 nM PSa-2 and 800 nM PSb-2 (5:5), 640 nM PSa-2 and 960 nM PSb-2 (4:6), 320 nM PSa-2 and 1280 nM PSb-2 (2:8), 0 nM PSa-2 and 1600 nM PSb-2 (0:10).

Discussion:

One can notice that the brightness of PSa band (Lane 1) decreases upon PSb addition (Lane 2) and no obvious component band is observed in Lanes 3, 4 and 5. With further excess amounts of PSb, the PSb band appears in Lane 6 and increases its brightness to the highest value in Lane 7. Because the DNA bands on the two sides of Lane 4 (i.e., Lanes 1, 2 and 3 versus Lanes 5, 6 and 7, respectively) are apparently symmetric, the PSa-to-PSb ratio of 5:5 is considered to be most suitable for the [2]GDA assembly, which is also consistent with the theoretical value.

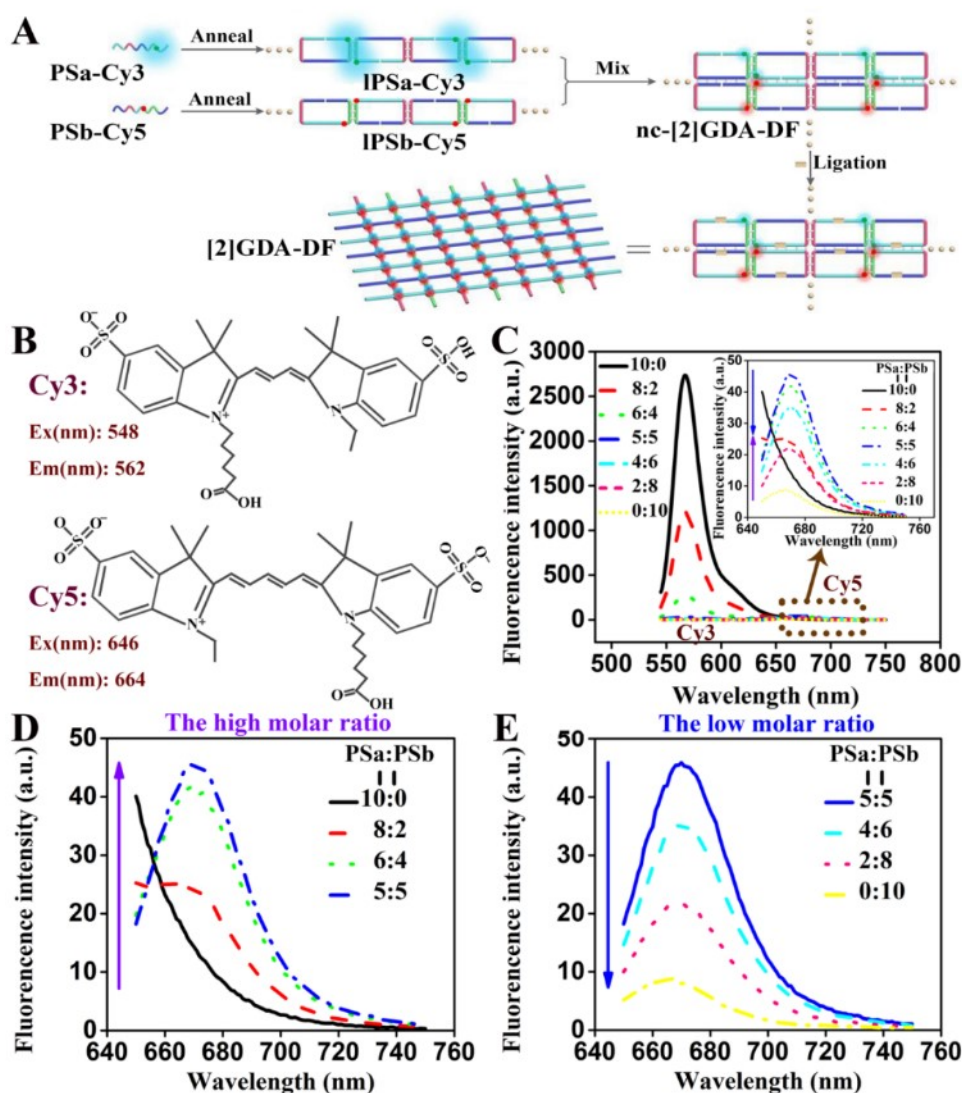


Figure S5. Fluorescence resonance energy transfer (FRET) analysis of [2]GDA-DF assembled at different molar ratios of PSa-2-Cy3/PSb-2-Cy5: (A) Schematic illustration of [2]GDA-DF assembly, accompanied by the relative position of Cy3 and Cy5. The two fluorophores are in the close proximity to each other. (B) Structural formulas of Cy3 and Cy5; (C) fluorescence emission spectra of [2]GDA-DFs assembled at different PSa-2-Cy3-to-PSb-2-Cy5 ratios. The part bounded by a dotted brown frame is enlarged in Inset, which describes the emission spectra of Cy5. (D) and (E) show the fluorescence spectra of Cy5 at the high ratio ranging from 10:0 to 5:5 and at the low ratio from 5:5 to 0:10, respectively. The samples were prepared using the same procedure as that adopted in **Figure S4**, but PSa-2-Cy3 and PSb-2-Cy5 were employed instead of the two label-free PSa-2 and PSb-2, respectively. The FRET measurement was performed as described in the section **SA.1**.

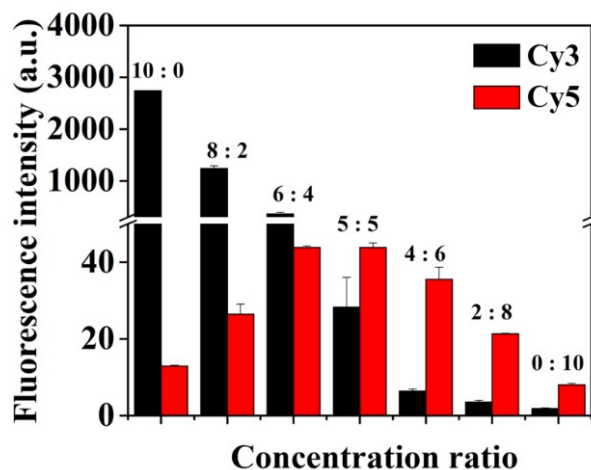


Figure S6. The fluorescence intensity of Cy3 at 567 nm and Cy5 at 672 nm recorded from [2]GDA-DF assembled at different molar ratios of PSa-2-Cy3/PSb-2-Cy5. The excitation wavelength was fixed at 525 nm (donor Cy3) and the emission range was collected from 545 nm to 750 nm. The corresponding fluorescence emission spectra are shown in **Figure S5**.

Discussion for Figure S5 and Figure S6:

The molar ratio of PSa-to-PSb is further explored by fluorescence resonance energy transfer (FRET) measurement to offer fully convincing evidence. For this purpose, PSa and PSb were labeled with Cy3 and Cy5, respectively, and the corresponding probes were called PSa-2-Cy3 and PSb-2-Cy5. The fluorescently dual-labeled nanostructure assembled from PSa-2-Cy3 and PSb-2-Cy5 is named [2]GDA-DF. As described in **Figure S5A**, in [2]GDA-DF, Cy3 and Cy5 were arranged at the predetermined position, and they are in close proximity to each other, which is close enough for efficient energy transfer from the photoexcited donor Cy3 to the acceptor Cy5. The molecular formulas of Cy3 and Cy5 are displayed in **Figure S5B**. At the excitation wavelength of Cy3, the fluorescence emission spectra of Cy3 and Cy5 (Inset) from [2]GDA-DF at different PSa-2-Cy3-to-PSb-2-Cy5 ratios are shown in **Figure S5C**. Moreover, the fluorescence spectra of Cy5 at the high ratio ranging from 10:0 to 5:5 and at the low ratio from 5:5 to 0:10 are presented in **Figures 5D** and **5E**, respectively. The corresponding fluorescence peak values are quantitatively shown in **Figure S6**. One can notice that, when decreasing the PSa-2-Cy3-to-PSb-2-Cy5 ratio but at a constant total concentration, the Cy3 fluorescence monotonically decreases because of the decrease of PSa-2-Cy3 concentration, while the Cy5 fluorescence increases first and then reaches the highest value at the 5-to-5 ratio, indicating the highest FRET efficiency. If the PSb-2-Cy5 concentration further increases, the Cy5 fluorescence does not increase but decreases, which is reasonable because the amount of energy transferred from donor dye of Cy3 is not enough strong to excite the excess Cy5 acceptors. Hence, the ratio of 5:5 is chosen as the optimized molar ratio of PSa-2-Cy3-to-PSb-2-Cy5 in the subsequent experiments.

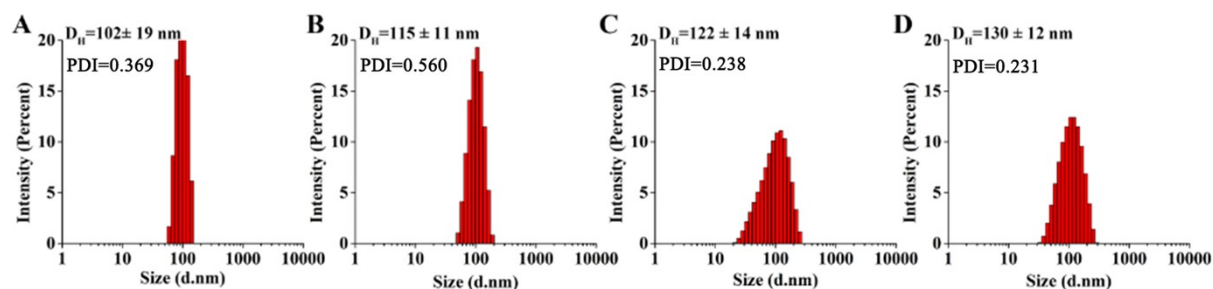


Figure S7. The DLS analysis of [2]GDA assembled from PSa-2 and PSb-2 at various concentrations. (A) 12.5 μ L of 0.8 μ M PSa-2 + 12.5 μ L of 0.8 μ M PSb-2. (B) 12.5 μ L of 1.6 μ M PSa-2 + 12.5 μ L of 1.6 μ M PSb-2. (C) 12.5 μ L of 2.4 μ M PSa-2 + 12.5 μ L of 2.4 μ M PSb-2. (D) 12.5 μ L of 3.2 μ M PSa-2 + 12.5 μ L of 3.2 μ M PSb-2. The final concentrations of each component in the four samples are 0.4 μ M, 0.8 μ M, 1.2 μ M and 1.6 μ M, respectively. The hydrodynamic diameter (D_H) and the polydispersity index (PDI) of each sample are given in the upper part. The same experimental process was adopted for the preparation of the four samples, which is described in the section of “The dynamic light scattering analysis of [2]GDA”.

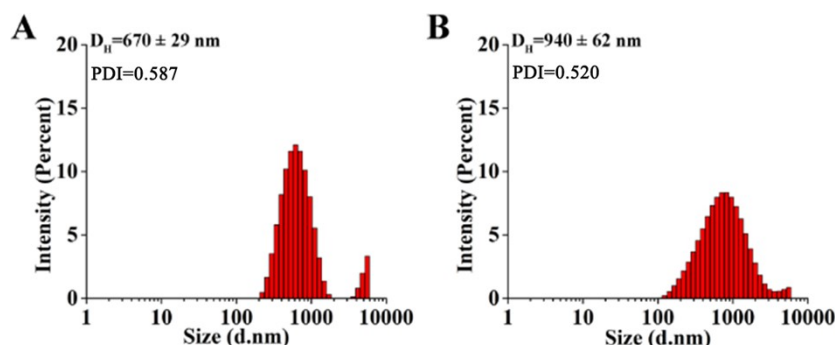


Figure S8. The DLS analysis of [2]GDA assembled from the high concentration of PSa-2 and PSb-2. (A) 12.5 μ L of 15 μ M PSa-2 + 12.5 μ L of 15 μ M PSb-2. (B) 12.5 μ L of 20 μ M PSa-2 + 12.5 μ L of 20 μ M PSb-2. The final concentrations of each building component in the two samples are 7.5 μ M and 10 μ M, respectively. The hydrodynamic diameter (D_H) and polydispersity index (PDI) of the two samples are shown in upper part. The same experimental process was adopted for the preparation of the two samples, which is described in the section of “The dynamic light scattering analysis of [2]GDA”.

Discussion for Figure S7 and Figure S8:

The size of [2]GDA can be controlled by changing the concentration of DNA building components. As shown in **Figure S7**, the hydrodynamic diameter of [2]GDA increases from 102 to 130 nm when increasing the concentration of building components from 0.4 to 1.6 μ M. However, if the building component concentration decreases to a very low value (e.g., 80 nM), [2]GDA was incapable of being detected by DLS. It is perhaps because the size of the products assembled from the low concentration of building components is too small to be measured. In contrast, as shown in **Figure S8**, if much higher concentration (e.g., 7.5 μ M and 10 μ M) of building components was used for the assembly, the hydrodynamic diameter of [2]GDA increases to the larger size (e.g., 670 nm and 940 nm).

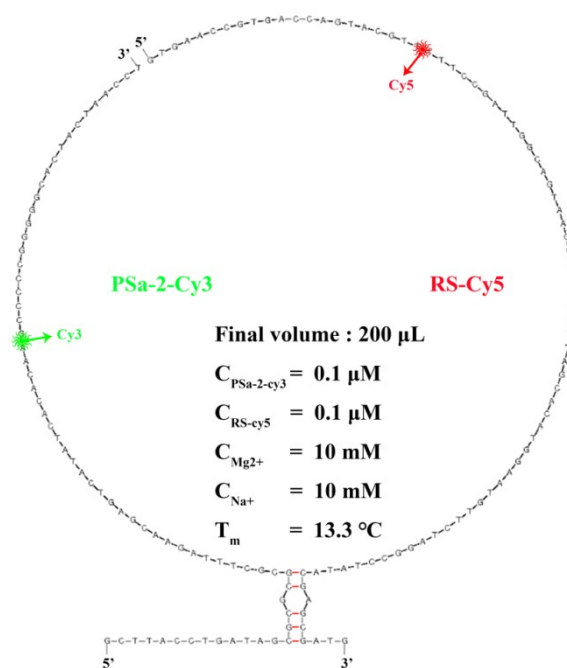


Figure S9. The secondary structure of PSa-2-Cy3/RS-Cy5 duplex predicted with the help of an online bioinformatic software (<http://unafold.rna.albany.edu/>). $C_{\text{PSa-2-Cy3}}$, $C_{\text{RS-Cy5}}$, $C_{\text{Mg}^{2+}}$ and C_{Na^+} indicate the final concentration of PSa-2-Cy3, RS-Cy5, Mg^{2+} and Na^+ in 200 μ L of solution, respectively. T_m means the melting temperature. It can be seen that PSa-2-Cy3 and RS-Cy5 cannot form the stable duplex at room temperature.

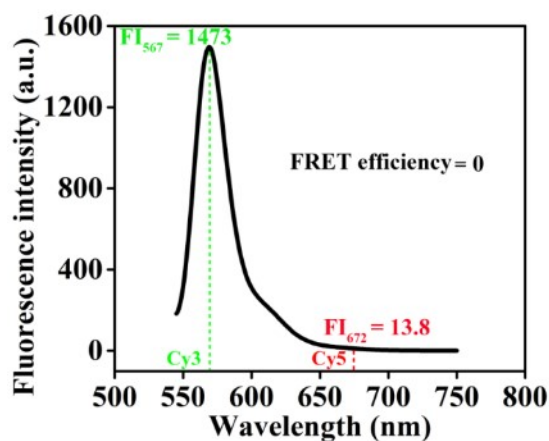


Figure S10. Fluorescence spectrum of the mixture of PSa-2-Cy3 and RS-Cy5 at an equal molar ratio. FI_{567} and FI_{672} denote the fluorescence intensity at 567 nm and 672 nm, respectively. The excitation wavelength was set as 525 nm (donor Cy3). The final concentration of each DNA component was 100 nM.

Experimental procedure:

A 2- μ L aliquot of 10 μ M PSa-2-Cy3, 2 μ L of 10 μ M RS-Cy5 and 20 μ L of 10 \times T4 DNA Ligase buffer were added to 176 μ L of ddH₂O and mixed well. The final concentration of each DNA strand was 100 nM. After annealing at 90 $^{\circ}$ C for 5 min and gradually cooling down to room temperature, the fluorescence spectrum of the resulting solution was collected from 545 nm to 750 nm with the excitation wavelength of 525 nm (corresponding to Cy3).

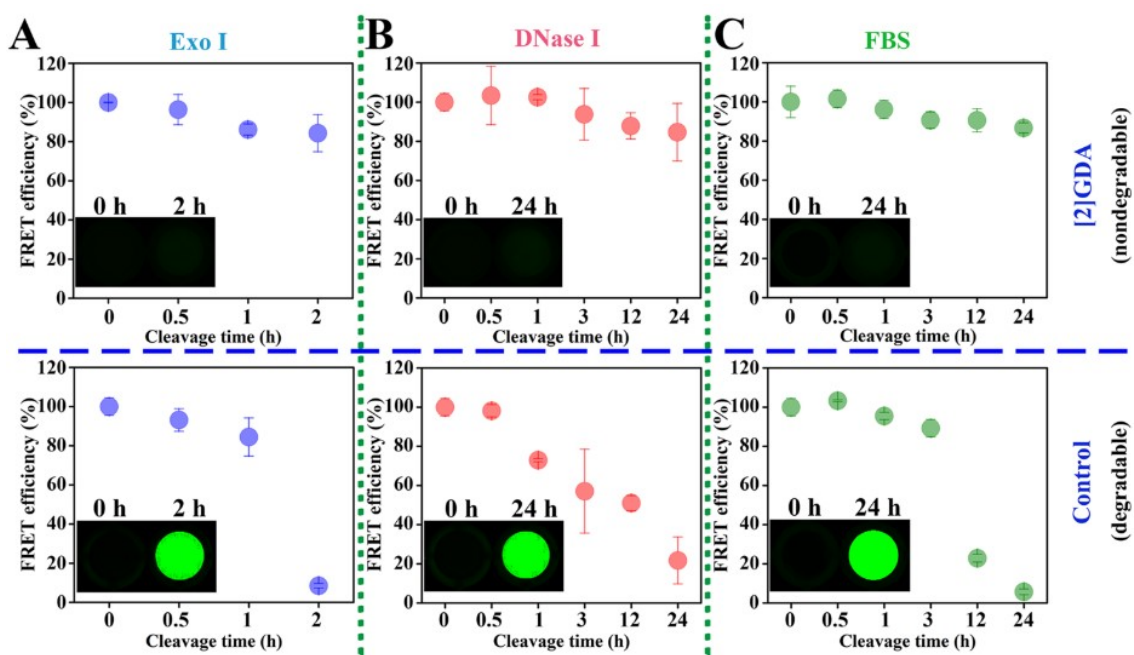


Figure S11. Fluorescence resonance energy transfer (FRET) analysis to evaluate the resistance of [2]GDA to enzymatic degradation in biological digestion solutions in the presence of Exo I (0.4 U/ μ L) (A), DNase I (3 U/mL) (B) or 10% FBS (C). The final concentration of each DNA component in each sample was about 710 nM. For the [2]GDA group (upper part), [2]GDA-DF was assembled from the intact PSa-2-Cy3 and intact PSb-2-Cy5 and then was treated with Exo I, DNase I or FBS, followed by the quantitative fluorescence measurement. However, for the control group (lower part), PSa-2-Cy3 and PSb-2-Cy5 were pre-treated with Exo I, DNase I or FBS under identical conditions and then used to assemble the [2]GDA-DF. The experimental procedures for preparing [2]GDA group are shown in the section of “Preparation of catenane-based grid-patterned DNA arrays (GDA)”. The FRET efficiency was estimated according to the method described in the section of SA.1. The insets are the Cy3 fluorescence-based pictures taken from the corresponding samples. Further quantitative evaluation of the resistance of [2]GDA to enzymatic degradation is described in Figure S12.

Experimental procedure:

Control groups in Figure S11A-C: When assessing the nuclease-degradation resistance, PSa-2-Cy3 degradation solution and PSb-2-Cy5 degradation solution were prepared in advance. Specifically, 2 μ L of 10 μ M PSa-2-Cy3 and 1.25 μ L of 10 \times T4 DNA Ligase buffer were added to 9.25 μ L of ddH₂O and mixed. The resulting solution (12.5 μ L) was annealed at 90 $^{\circ}$ C for 5 min and allowed to cool down to room temperature slowly. Then, 0.25 μ L of DNase I and 1.4 μ L of 10 \times DNase I buffer were added, followed by incubation at 37 $^{\circ}$ C for different time periods (0–24 h). The final concentration of DNase I was 3 U/mL. Subsequently, the heat inactivation of DNase I at 75 $^{\circ}$ C for 20 min was performed, followed by cooling slowly down to room temperature. The resulting solution was called *PSa-2-Cy3 degradation solution*. *PSb-2-Cy5 degradation solution* was prepared according to the same procedure. Afterwards, the two solutions were mixed (about 28 μ L) and incubated at room temperature for 30 min. After adding 0.5 μ L of T4 DNA Ligase, the ligation was allowed to proceed at 16 $^{\circ}$ C for 1 h. Finally, the final assembly solution (28 μ L) was diluted with 1 \times T4 DNA Ligase buffer to 200 μ L, and the FRET was measured as described in the section SA.1.

The resistance of control groups to FBS or Exo I was explored according to the same procedure, but 0.25 μ L of ddH₂O and 1.4 μ L of FBS (or 0.25 μ L of Exo I and 1.4 μ L of

10×Exo I buffer) was used instead of 0.25 μL of DNase I and 1.4 μL of 10×DNase I buffer, respectively. The final concentrations of FBS and Exo I were 10% FBS and 0.4 U/ μL , respectively.

Discussion:

The stability of GDA against enzymatic degradation was also evaluated by measuring FRET efficiency of [2]GDA-DF. Owing to the ability to specifically hydrolyze single-stranded DNA from the terminal of 3' to 5', Exo I (e.g., 0.4 U/ μL , 30-min incubation;^[S4] or 0.25 U/ μL , 1-h incubation^[S5]) was often used to assess the nuclease stability of DNA probes. Similarly, the DNase I treatment (0.5-5 U/mL, about 60 min) is also considered as the ideal strategy to characterize the resistance of DNA nanostructures to nuclease degradation^[S6] because it is capable of efficiently digesting single- and double-stranded DNA and its level in serum is 0.36 U/mL.^[S7] To convincingly demonstrate the unique advantages, the biological stability of [2]GDA-DF was studied under much harsher conditions (i.e., treated by 2-h incubation in 0.4 U/ μL Exo I solution or 24-h incubation in 3 U/mL DNase I solution), and the structural integrity of resulting DNA nanostructures was evaluated by measuring the FRET signal change. Excitingly, as shown in **Figure 11A** and **11B**, more than 80% FRET signal of [2]GDA-DF is retained regardless of nuclease nature and incubation time, while no detectable Cy3 fluorescence emits from the corresponding solution (Inset images), indicating the desirable resistance of [2]GDA to nuclease degradation. In contrast, less than 10% (or 20%) of FRET signal is detected from the control group consisting of DNA components pre-treated with Exo I (or DNase I) before self-assembly. Similarly, the fluorescence images of corresponding solutions (Insets of control groups) also confirm the substantial digestion of DNA components since very high Cy3 fluorescence is observed that indicates the failure of FRET from Cy3 to Cy5.

Taking into account that the systemic administration of DNA nanostructures often results in the rapid clearance in blood because of nuclease digestion and thereby hinders the transition to practical applications in biomedical imaging and therapy,^[S7b, S8] the serum stability of [2]GDA was further assessed by incubating in 10% fetal bovine serum (FBS). Similar to the results of **Figure 11A** and **Figure 11B**, no substantial decrease in the FRET signal of [2]GDA-DF is detected over the entire 24-h duration (**Figure 11C**) compared with its control, which is consistent with Cy3 fluorescence-based imaging experiments (Inset), implying the sufficient stability of [2]GDA in serum solution. Since the PSa-2-Cy3 (or PSb-2-Cy5) alone can be considerably digested by nucleases, that no obvious change in the fluorescence signal of [2]GDA-DF is induced by the degradation treatment demonstrates that almost all fluorescently-labeled DNA components participate the assembly process, which agrees well with the high assembly efficiency determined by **Figure S1**. The stability of [2]GDA against nuclease degradation and its efficient assembly are further confirmed by nPAGE analysis as shown in **Figure S12**. Meanwhile, one can notice that the grayscale signal from the gel band is slightly higher than the corresponding FRET signal shown in **Figure 11**. It seems to be because, even if some Cy3 donors and Cy5 acceptors are separated from each other and compromise the FRET signal, the component strands of [2]GDA is not sufficiently digested and can appear in the gel band.

To further validate the impressive nuclease stability of [2]GDA and elucidate the contribution of palindromic fragments to the structural features, two common DNA counterparts (rPSa-2 and rPSb-2) were designed only by rearranging the base order in a random fashion to destroy the palindromic structure but not changing the base number/nature. Then, their nuclease degradation resistance was evaluated separately or together according to the experimental procedure described in **Figure S12**. As shown in **Figure S13**, the stability of

[2]GDA against FBS degradation is enhanced by at least two orders-of-magnitude compared with common DNA counterparts. Moreover, the difference in the stability between [2]GDA and the counterparts in Exo I solution and DNase I solution is too large to be estimated. More information is presented in Figure S13.

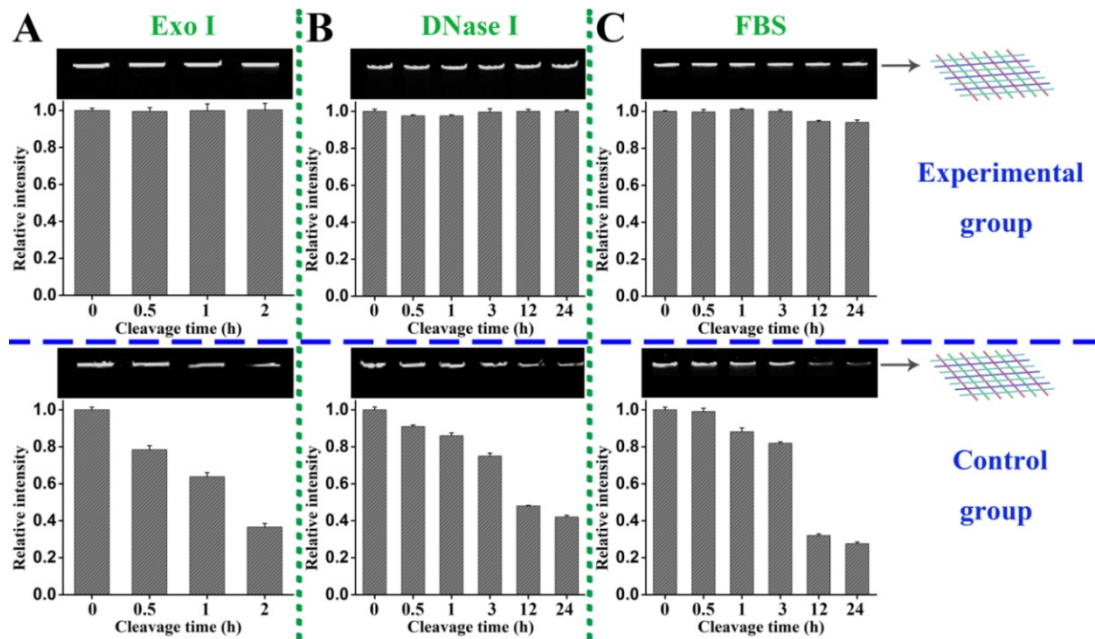


Figure S12. The nPAGE analysis to demonstrate the resistance of [2]GDA to enzymatic degradation by subjecting to biological media in the presence of (A) Exo I (0.4 U/ μ L), (B) DNase I (3 U/mL) or (C) 10% FBS. The final concentration of each DNA component in each sample was about 710 nM. For the experimental group (upper part), [2]GDA was assembled from the intact PSa-2 and PSb-2, and the residues after digestion were quantified by nPAGE analysis. However, for the control group (lower part), PSa-2 and PSb-2 were pre-treated by Exo I, DNase I or FBS under identical conditions and then employed to prepare the [2]GDA, followed by nPAGE analysis.

Experimental procedure:

The experimental procedure is similar to that described in **Figure 11**, but label-free PSa-2 and label-free PSb-2 were instead employed. An 8- μ L aliquot of the final assembling solution was analyzed by nPAGE analysis. The fluorescence intensity (FI) of gel bands was quantified by employing Image J. The relative fluorescence intensity (Relative intensity) at various time points was estimated from FI_t/FI_0 , where FI_t and FI_0 are the fluorescence intensity of gel bands at a given time period and 0 h, respectively. In addition, FI_0 is defined as 1.

Discussion:

The nPAGE analysis show that no obvious change in the gel band of [2]GDA is detected even though treated with the high concentration of Exo I for a long time (2 h), highly-active DNase I or FBS for 24 h, manifesting the impressive biological stability of [2]GDA. If PSa-2 and PSb-2 were pretreated with Exo I, DNase I or FBS, the band intensity of [2]GDA substantially decreases with the increment of incubation time (e.g., 24-h incubation in DNase I solution or FBS solution) and even is less than 40% within a short time, for example, for 2-h treatment with Exo I (seen in the control group). The measured data from control group demonstrate the enzymatic degradation of DNA components alone. Given this, the assembly efficiency of [2]GDA is every high since no obvious degradation occurs in the Exo I, DNase I or FBS-containing solutions. Moreover, as shown in **Figure S13**, if the bases in PSa-2 and PSb-2 are rearranged to destroy the palindromic fragments, the resulting strands can be completely digested within a very short time (e.g., less than 30 min by Exo I). These experimental results demonstrate that the palindromic fragments introduced into DNA

components, especially the dual-palindromic hybridization (longitudinal and perpendicular)-based assembly process, can substantially enhance the degradation resistance of nucleic acid components even if the nature and number of their bases are not changed.

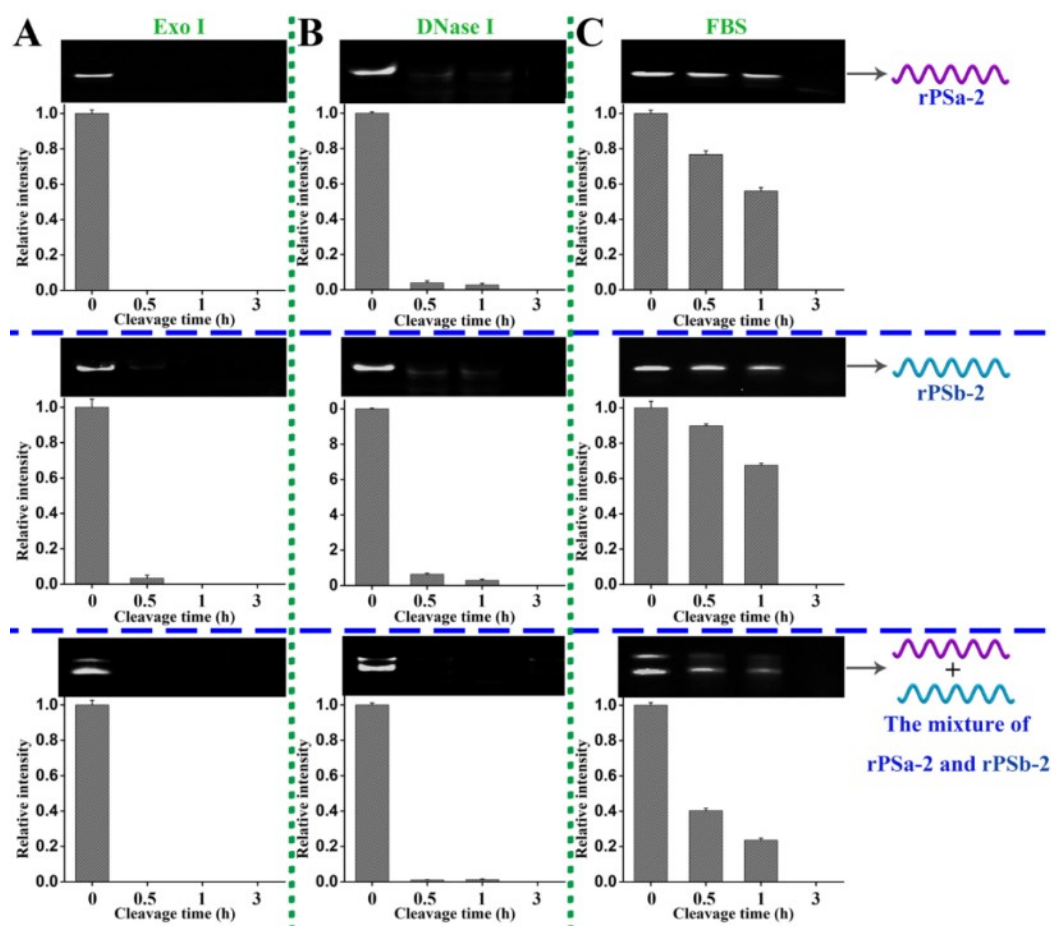


Figure S13. The susceptibility of rPSa-2 (upper panel), rPSb-2 (middle panel) and the mixture of rPSa-2 and rPSb-2 (lower panel) to enzymatic degradation, which was characterized by nPAGE analysis. The DNAs were incubated with Exo I (0.4 U/ μ L) (A), DNase I (3 U/mL) (B) and 10% FBS (C) for different time periods at 37 °C. The final concentration of each DNA component in the samples was about 710 nM. The fluorescence intensity (FI) of gel bands were quantified by employing Image J, and FI of DNA band at 0-h incubation is defined as 1. More details are seen in **Figure S12**.

Experimental procedure:

A 2- μ L aliquot of 10 μ M rPSa-2 and 2.5 μ L of 10 \times T4 DNA Ligase buffer were added to 20.5 μ L of ddH₂O and mixed well. The resulting 25- μ L solution was annealed at 90 °C for 5 min and allowed to cool down to room temperature slowly. Then, 0.5 μ L of DNase I and 2.8 μ L of 10 \times DNase I buffer were added (the final volume, 28 μ L), followed by incubation at 37 °C for different time periods (0–3 h). Finally, the heat inactivation of DNase I at 75 °C for 20 min was performed. The final concentration of DNase I was 3 U/mL.

The susceptibility of rPSa-2 to FBS or Exo I was explored according to the same procedure as that described above, but 0.5 μ L of ddH₂O and 2.8 μ L of FBS (or 0.5 μ L of Exo I and 2.8 μ L of 10 \times Exo I buffer) was used instead of 0.5 μ L of DNase I and 2.8 μ L of 10 \times DNase I buffer, respectively. The final concentrations of FBS and Exo I were 10% and 0.4 U/ μ L, respectively. The susceptibility of rPSb-2 to DNase I, FBS and Exo I was explored according to the same procedure.

To investigate the biological stability of the mixture of rPSa-2 and rPSb-2, 2.5 μ L of 10 \times T4 DNA Ligase buffer and equal amount of rPSa-2 and rPSb-2 (2 μ L, 10 μ M) were added to 18.5

μL of ddH_2O and mixed well. The subsequent processes were similar to those described above.

Discussion:

rPSa-2 is a single-stranded DNA without the palindromic domain. It was designed to have the same number of each of four bases (A, T, G and C) as PSa-2, but the bases were arranged in a random fashion. Similarly, rPSb-2 is different from PSb-2 despite the same base nature and number. Thus, rPSa-2 and rPSb-2 have no the stable secondary structure and cannot interact with each other. As shown in **Figure S13**, rPSa-2, rPSb-2 or the mixture of rPSa-2 and rPSb-2 is completely digested by Exo I, DNase I or FBS by incubation for 3 h and even much shorter time, suggesting that, after rearranging the bases of palindromic fragments in different orders, the resulting DNA strands are much more susceptible to enzymatic degradation. Clearly, the nuclease-degradation resistance of [2]GDA is based on the palindrome-based assembly of DNA components. To perform quantitative evaluation, the degradation resistance of [2]GDA is defined as $(a/b) \times 24/t$, where a indicates the relative intensity (RI) of [2]GDA at 24-incubation (the upper panel of **Figure S12C**) and b denotes the RI of rPSa-2/rPSb-2 mixture (equaling to common DNA strands) at t-h incubation. Along this line, estimated from the measured data at 0.5- and 1-h incubation (the bottom panel of **Figure S13C**), the average stability of [2]GDA in FBS solution is enhanced by at least two orders of magnitude compared with common DNA counterparts. Worthy of mention is that, the stability of [2]GDA in both Exo I solution and DNase I solution is too high to be estimated because it is hardly degraded under given conditions, which is different from its counterpart, rPSa-2/rPSb-2 mixture, that is almost completely digested.

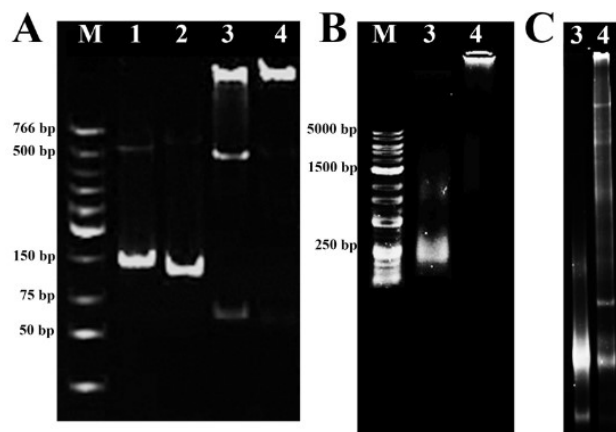


Figure S14. The characterization of [2]GDA-1 assembled from PSa-1 and PSb-1. (A) nPAGE image: Lane 1, lPSa-1; Lane 2, lPSb-1; Lane 3, nc-[2]GDA-1; Lane 4, [2]GDA-1. (B) Agarose gel electrophoresis (AGE) analysis of Samples 3 and 4. (C) dPAGE analysis of Samples 3 and 4. The DNA products were assembled as depicted in the section of “Preparation of catenane-based grid-patterned DNA arrays (GDA)”, while the gel electrophoresis analyses were carried out as shown in the section of “Gel electrophoresis”.

Discussion:

The clear band with about 150 bp appears in Lane 1 and in Lane 2, demonstrating the self-assembly of both lPSa-1 and lPSb-1 by the palindromic fragment-based hybridization because PSa-1 or PSb-1 is as a DNA strand with only 59 bases. A main band with the very slow electrophoretic mobility (EM) is observed in Lane 3 and only one band with the slower EM appears in Lane 4, certifying the formation of nc-[2]GDA-1 and [2]GDA-1 with the high molecular weight (MW). Besides, two additional DNA bands with the fast EM are detected in Lane 3, implying the polydisperse structures of nc-[2]GDA-1 compared with [2]GDA-1. It should be attributed to the lower structural stability because there are many nicks in nc-[2]GDA-1.^[4]

To verify further the difference between nc-[2]GDA-1 and [2]GDA-1, Samples 3 and 4 were characterized by AGE analysis capable of sensing the change in DNA materials with relative high MW. As shown in **Figure S14B**, the fast-moving bands appear in Lane 3, while very slow and sharp bands are observed in Lane 4. The difference in band mobility between the two lanes demonstrates that the structure of nc-[2]GDA-1 is remarkably different from [2]GDA-1. The former is prone to form small DNA assemblies (about 250 bp) because of the existence of the nicks and the latter can self-assemble into very high-molecular-weight architectures where the components are tightly catenated to each other due to the ligation-mediated cyclization.

The dPAGE analysis further reveals the importance of the sealing of the nicks for the assembly of large catenation-based DNA architecture. As shown in **Figure S14C**, a very wide main band with high EM is detected in Lane 3. In contrast, there is a main band with the high degree of gel electrophoresis retardation in Lane 4. Nevertheless, a serial of DNA bands with various molecular weights are still observed, which is considerably different from Lane 4 (expected [2]GDA) of **Figure S1B**. Clearly, the desirable high-molecular-weight [2]GDA cannot be efficiently assembled from PSa-1 and PSb-1 regardless of whether the ligase is used or not. Presumably, after the two DNA strands were shortened by removing 18 bases, the considerable amount of DNA components cannot be efficiently cyclized or catenated to each other even if the ligase is used to seal the nicks and thereby the assembled complexes are easily denatured into the linear single-stranded (ss) components, circular uncatenated ss-DNA rings and/or low-catenation-based structures.

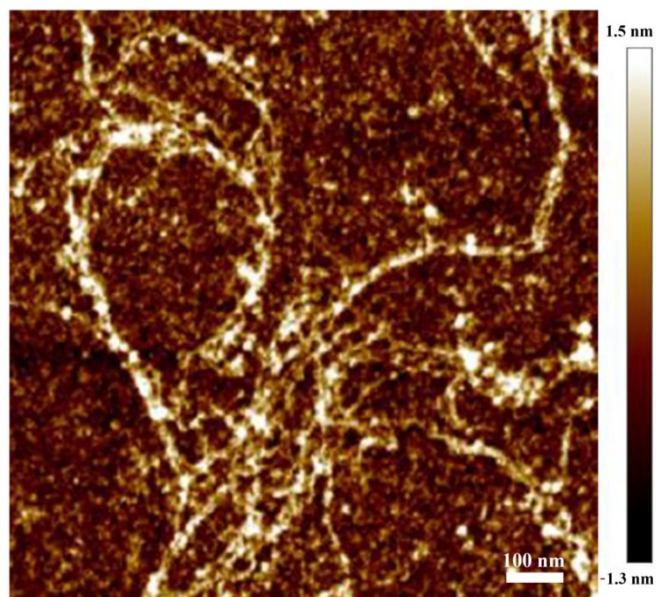


Figure S15. AFM image of [2]GDA-1 assembled from PSa-1 and PSb-1. The assembly was performed according to the procedure depicted in the section of “Preparation of catenane-based grid-patterned DNA arrays (GDA)”, while AFM imaging was performed as described in the section of “AFM imaging”. As demonstrated by the morphology and physical size, the assembled products are the irregularly branched DNA nanostructures where there possibly are uncyclized hybridized DNA components, cyclized ss-DNA rings or low-catenation-based DNA complexes.

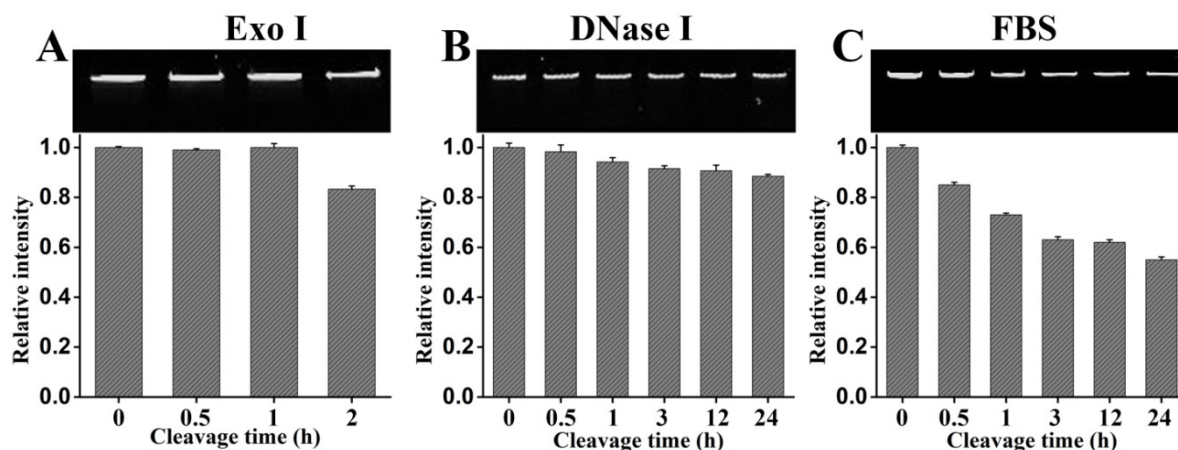


Figure S16. nPAGE analysis of the resistance of [2]GDA-1 assembled from PSa-1 and PSb-1 to protease digestion. [2]GDA-1 was treated by incubation with (A) Exo I (0.4 U/ μ L), (B) DNase I (3 U/mL) or (C) 10% FBS at 37 °C. The gel bands of [2]GDA-1 were fluorescently quantified by Image J, where the fluorescence intensity of DNA bands at 0-h incubation is defined as 1. The reaction solutions were prepared as described in the section SA.1, while the gel electrophoresis was performed as shown in the section of “Gel electrophoresis”.

Discussion:

The measured data demonstrate that [2]GDA-1 is degraded by Exo I, DNase I and FBS to varying degrees, which is quite different from the measured data from [2]GDA-2 (Experimental group in **Figure S12**) assembled for PSa-2 and PSb-2. Specially, a slight degradation of [2]GDA-1 is observed in the presence of Exo I, which is distinctly different from the complete degradation of rPSa-2/rPSb-2 mixture described in **Figure S13**. It is reasonable because the palindromic fragments in [2]GDA-1 can interact with each other, forming the double-stranded fragments that is not digested by Exo I. Similarly, after incubation with DNase I (e.g., 24 h), a low but detectable degradation is detected. Especially, only less than 60% of [2]GDA-1 is retained after incubation with 10% FBS for 24 h, demonstrating a considerable decrease in the stability against enzymatic degradation after shortening the DNA building components.

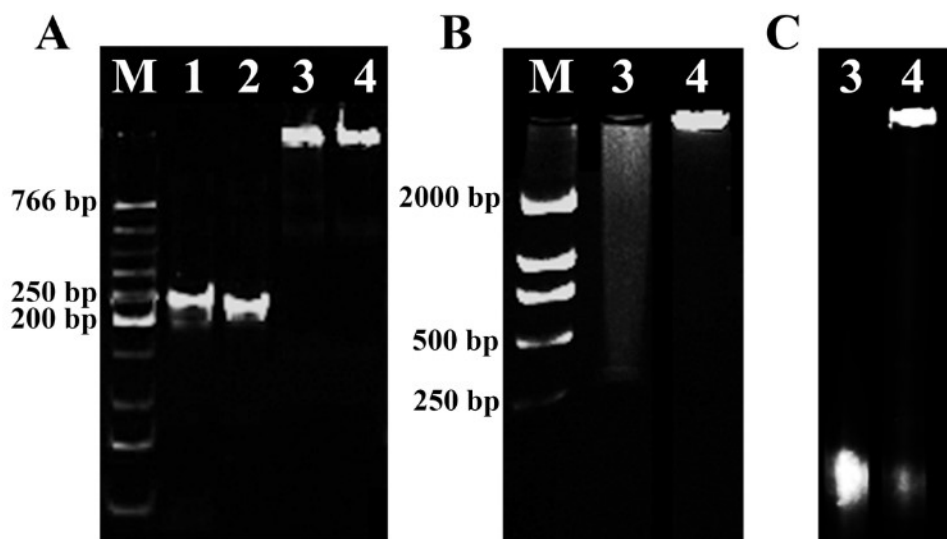


Figure S17. The characterization of [2]GDA-3 assembled from PSa-3 and PSb-3. (A) nPAGE image: Lane 1, IPSa-3; Lane 2, IPSb-3; Lane 3, nc-[2]GDA-3; Lane 4, [2]GDA-3. (B) Agarose gel electrophoresis (AGE) analysis of Samples 3 and 4. (C) dPAGE analysis of Sample 3 and 4. The DNA products were assembled as depicted in the section of “Preparation of catenane-based grid-patterned DNA arrays (GDA)”, while the gel electrophoresis analyses were carried out as shown in the section of “Gel electrophoresis”.

Discussion:

One can notice that the clear band with about 250 bp appears in Lane 1 and in Lane 2, demonstrating the generation of IPSa-3 and IPSb-3 (each with 77 bases) on the basis of the palindromic fragment-based hybridization. One band with no obvious electrophoretic mobility shift appears in Lane 3 or Lane 4, certifying the formation of nc-[2]GDA-3 and [2]GDA-3 with a high molecular weight.

To verify the difference between nc-[2]GDA-3 and [2]GDA-3, samples 3 and 4 are further characterized by AGE. As shown in **Figure S17B**, a considerably-widened band is observed in Lane 3, implying the large polydispersity of nc-[2]GDA-3 structures. In contrast, only one clear and substantially retarded band appears in Lane 4, suggesting the efficient assembly of [2]GDA-3 and low size polydispersity. These images prove that the ligation-cyclization can promote the synthesis of [2]GDA-3.

Nevertheless, the dPAGE analysis demonstrates that some unwanted byproducts are generated from PSa-3 and PSb-3 even in the presence of ligase. As shown in **Figure S17C**, only one DNA band is observed in Lane 3 and moves quickly, implying that all the nc-[2]GDA-3 assemblies are separated into single strands under denaturing conditions because of the nicks existing in the assembled structures. Meanwhile, it can be also noticed that there are two bands in Lane 4, one main band and the other minor one. Although the very slow main band demonstrates the formation of [2]GDA-3, the fast minor band indicates some unsealed DNA components in [2]GDA-3. It is probably because the spherical structure of [2]GDA-3 (**Figure S18**) prevents the interior DNA components from interacting with external large biospecies and causes the limited access of T4 DNA Ligase to the nicks inside nanostructures, leading to the failure of some nick-sealing reactions. Overall, these electrophoresis images demonstrate that the DNA components with the longer sequences are not quite suitable for the assembly of catenane-based grid-patterned DNA crystals (GDA).

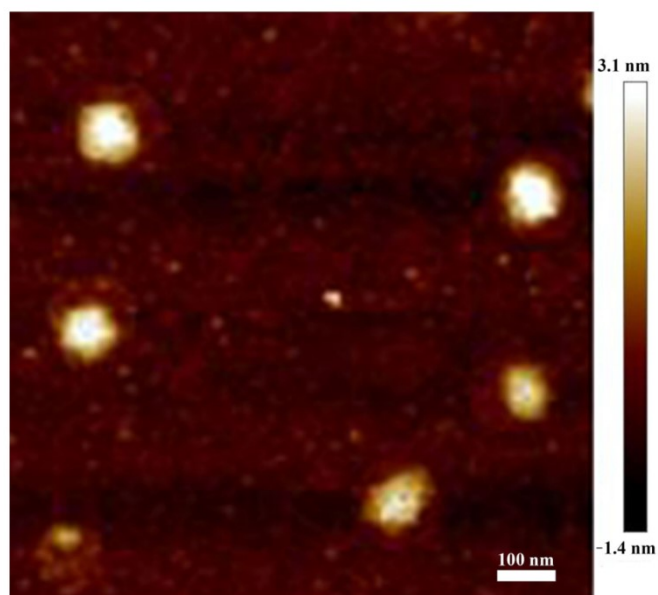


Figure S18. Atomic force microscopy (AFM) image of [2]GDA-3 assembled from PSa-3 and PSb-3. The assembly was performed according to the procedure depicted in the section of “Preparation of catenane-based grid-patterned DNA arrays (GDA)”, while AFM imaging was performed as described in the section of “AFM imaging”. As demonstrated by the morphology and physical size, the as-assembled [2]GDA-3 products are typical well-dispersed spherical nanostructures with an average diameter of 138 ± 19 nanometers ($n=91$).

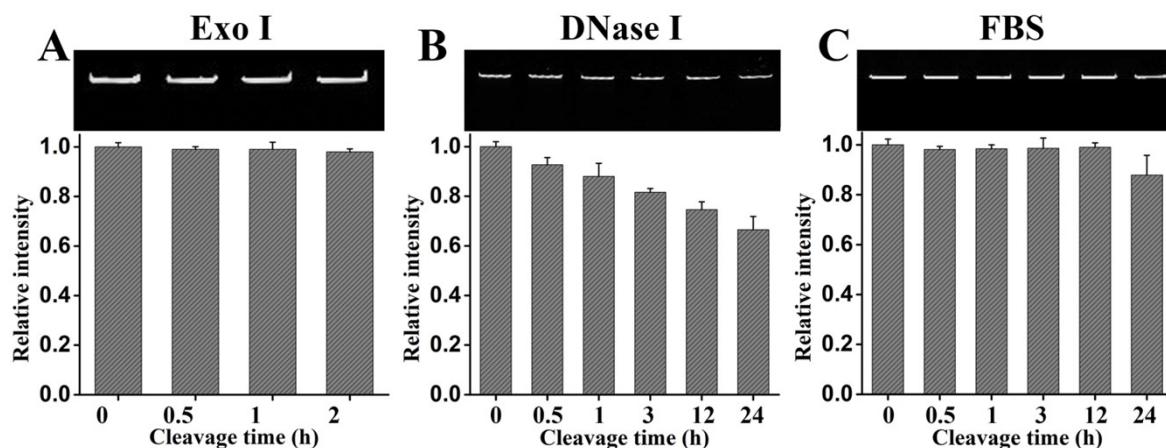


Figure S19. nPAGE analysis of the resistance of [2]GDA-3 assembled from PSa-3 and PSb-3 to protease digestion: (A) Exo I (0.4 U/ μ L), (B) DNase I (3 U/mL) and (C) 10% FBS, at 37 °C. Gel bands of [2]GDA-3 were fluorescently quantified by Image J, where the fluorescence intensity of DNA band at 0-h incubation is defined as 1. The reaction solutions were prepared as described in the section SA.1, while the gel electrophoresis was performed as shown in the section of “Gel electrophoresis”.

Discussion:

The measured data demonstrate that, although no obvious change in DNA band exposed to Exo I (panel A) is detected because there are the double-stranded fragments resulting from the hybridization between palindromic domains, [2]GDA-3 is degraded by FBS and especially by DNase I. For example, more than 30% of [2]GDA-3 is digested after incubation with DNase I for 24 h, demonstrating that the resistance of [2]GDA-3 to enzymatic degradation is compromised compared with [2]GDA-2 (Figure S12B).

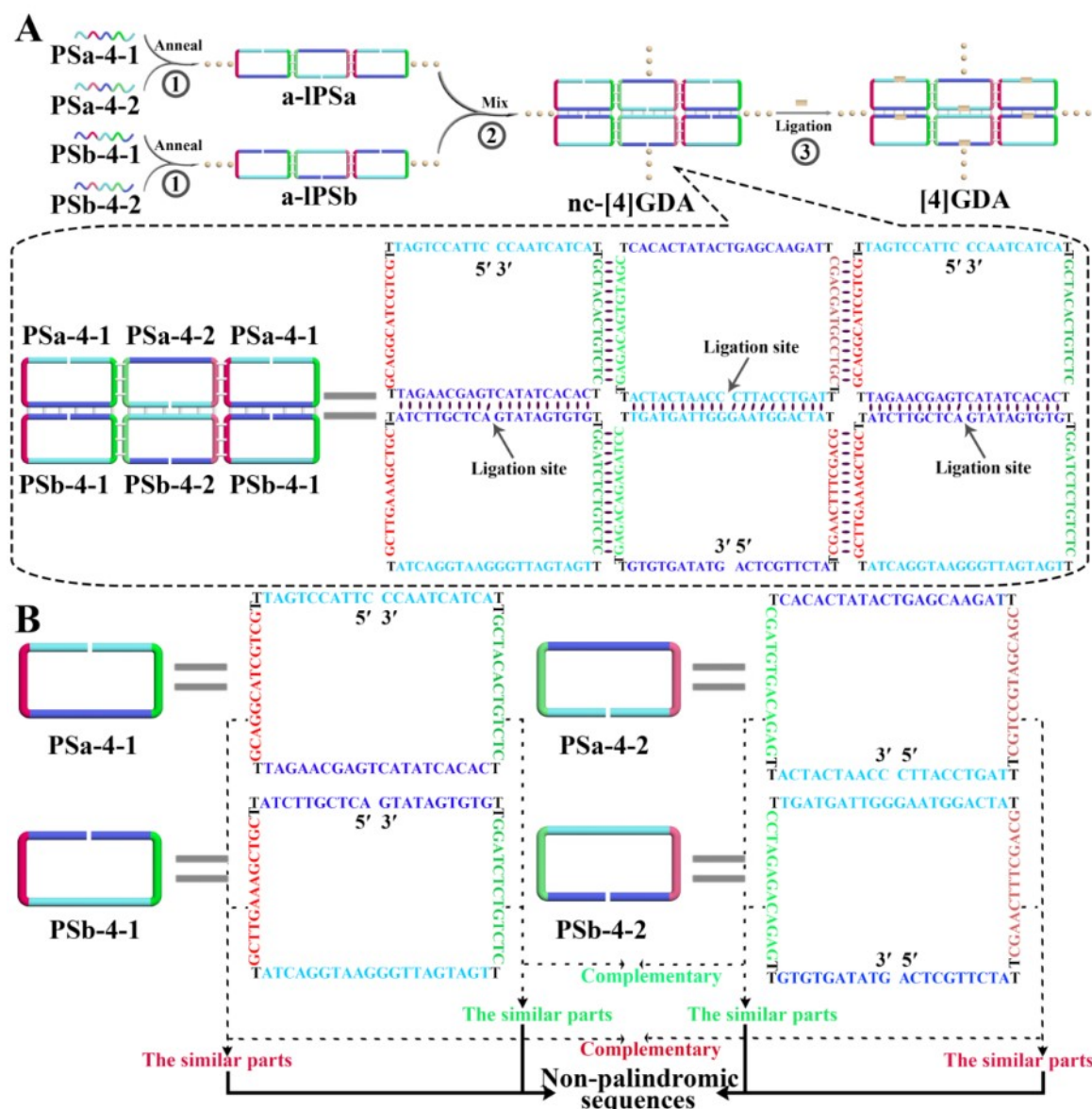


Figure S20. (A) Schematic illustration of the construction of [4]GDA and Watson-Crick base pairing interaction between DNA components. (B) The description of functional domains of PSa-4-1, PSa-4-2, PSb-4-1 and PSb-4-2.

Experimental procedure:

The experimental procedures are described as follows: **Step ①: Solution 1:** 12.5 μL of 1 \times T4 DNA Ligase buffer containing PSa-4-1 and PSa-4-2 was heated at 90 $^{\circ}\text{C}$ for 5 min and then allowed to cool down to room temperature. The assembled material is dubbed a-IPSa because PSa-4-1 and PSa-4-2 are alternately aligned into the linear DNA complex. **Solution 2:** 12.5 μL of 1 \times T4 DNA Ligase buffer containing PSb-4-1 and PSb-4-2 was heated at 90 $^{\circ}\text{C}$ for 5 min, followed by cooling down to room temperature. Similarly, PSb-4-1 and PSb-4-2 are alternately aligned into another linear complex, a-IP Sb. **Step ②:** Solution 1 and Solution 2 were mixed thoroughly and kept at room temperature for 30 min. **Step ③:** 0.5 μL of T4 DNA Ligase was added and incubated for 1 h at 16 $^{\circ}\text{C}$ for ligation reaction. The final volume of resulting solution is 25 μL , and each DNA component concentration is 800 nM.

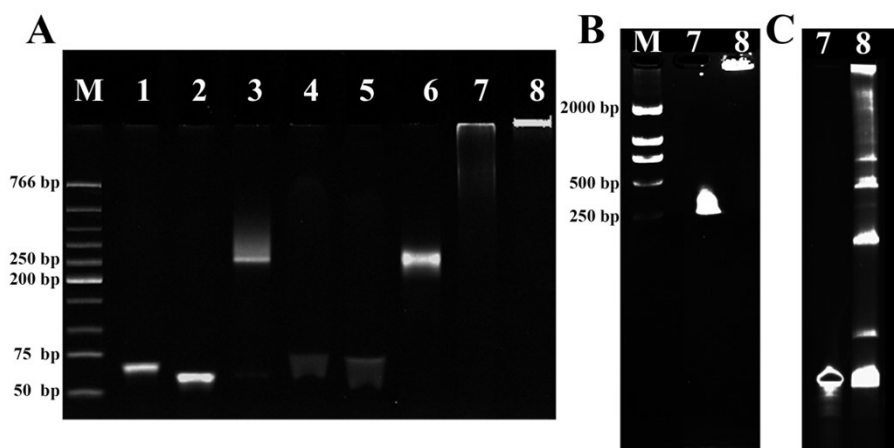


Figure S21. The characterizations of [4]GDA assembled from PSa-4-1, PSa-4-2, PSb-4-1 and PSb-4-2. (A) nPAGE image: Lane 1, PSa-4-1; Lane 2, PSa-4-2; Lane 3, a-IPSa; Lane 4, PSb-4-1; Lane 5, PSb-4-2; Lane 6, a-IP Sb; Lane 7, nc-[4]GDA; Lane 8, [4]GDA. (B) Agarose gel electrophoresis (AGE) analysis of samples 7 and 8. (C) dPAGE analysis of samples 7 and 8.

Experimental procedure:

Samples 1, 2, 4 and 5 were prepared by diluting PSa-4-1, PSa-4-2, PSb-4-1 and PSb-4-2 to 25 μ L with of 1 \times T4 DNA Ligase buffer, respectively, followed by heating at 90 $^{\circ}$ C for 5 min and then cooling down to room temperature. For preparation of sample 3 (or sample 6), the mixture of PSa-4-1/PSa-4-2 (or PSb-4-1/PSb-4-2) at an equal molar ratio was diluted to 25 μ L with 1 \times T4 DNA Ligase buffer and annealed at 90 $^{\circ}$ C for 5 min, followed by cooling down to room temperature. The resulting products in Samples 3 and 6 were called a-IPSa and a-IP Sb, respectively. Sample 7 was prepared by mixing a-IPSa with a-IP Sb, while Sample 8 was prepared according to the same procedure but with ligase-based cyclization. The final concentration of each DNA strand in all samples is 800 nM. The gel electrophoresis was performed as shown in the section of “Gel electrophoresis”.

Discussion:

As shown in **Figure S21A**, compared with the single-stranded components in Lanes 1, 2, 4 and 5 (each of them with 72 bp), the slow band (about 250 bp) appears in Lane 3 and Lane 6, indicating the formation of a-IPSa and a-IP Sb. The much slower smear band is observed in Lane 7, demonstrating the generation of nc-[4]GDA with a wide MW distribution. The appearance of a bright and sharp band in Lane 8 demonstrates the formation of [4]GDA with a narrow size distribution, implying that the ligation-based cyclization improves the catenation-based assembly efficiency of nanostructure. Moreover, as shown in **Figure S21B**, the [4]GDA band (Lane 8) does not exhibit an obvious change in electrophoretic mobility even by AGE analysis. In contrast, the substantial gel mobility shift is detected for nc-[4]GDA (Lane 7) under identical conditions, demonstrating that the nicks causes the structural instability of catenation-based assembled DNA products.

Nevertheless, as shown in Lane 8 of **Figure S21C**, the dPAGE analysis demonstrate that [4]GDA is denatured into several bands of various sizes, indicating that the structure of [4]GDA is very fragile under the denaturing conditions and DNA components is efficiently catenated to each other during the assembly. One only band with the high gel mobility is observed in Lane 7, demonstrating that all nc-[4]GDAs are denatured into short stands. It is reasonable because nc-[4]GDAs were not subjected to the ligase-based nick sealing treatment.

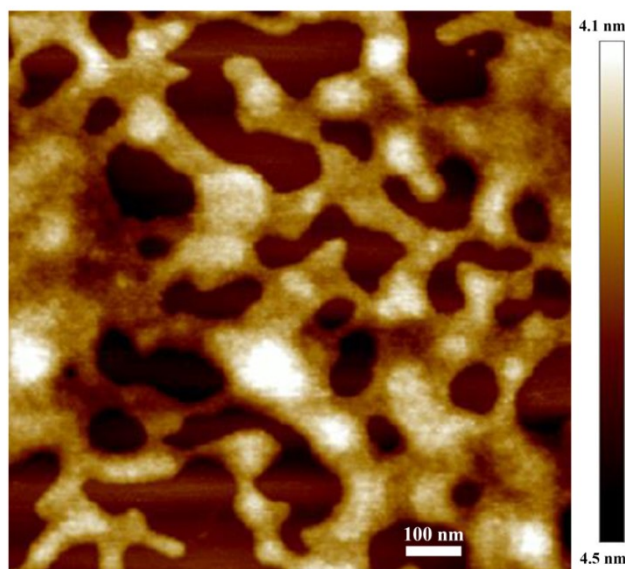


Figure 22. Atomic force microscopy (AFM) image of [4]GDA. One can notice that the width of DNA backbones in [4]GDA varies from tens to hundreds nanometers, the height (about 6 nm) is much higher than [2]GDA (**Figure 1D**), and the space between DNA backbones is very small, indicating the sterically crowded conformations that seemingly is unfavourable for the ligation-mediated catenation of DNA components. The assembly of DNA nanostructures was carried out as depicted in **Figure S20**.

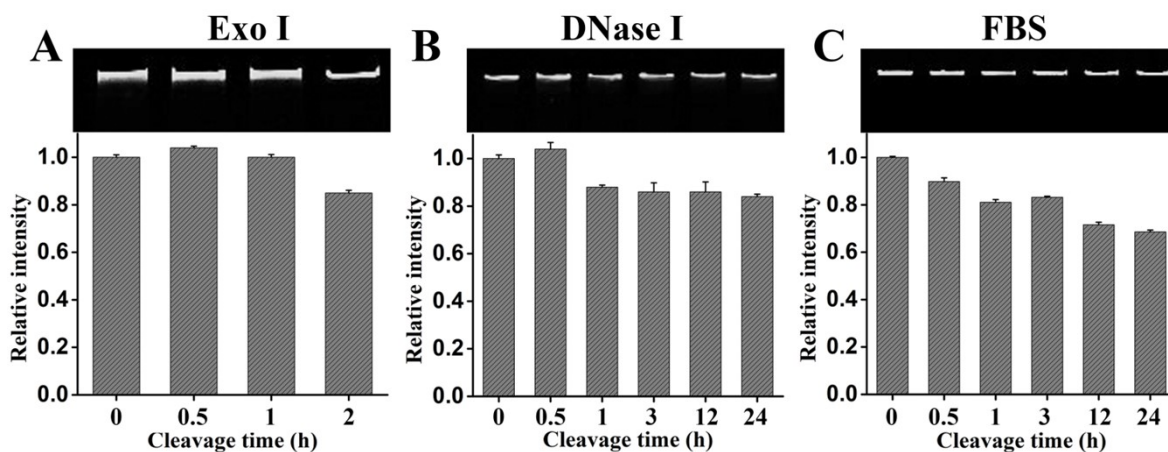


Figure S23. nPAGE analysis of the resistance of [4]GDA to nuclease degradation: (A) Exo I (0.4 U/ μ L), (B) DNase I (3 U/mL) and (C) 10% FBS, at 37 °C. Gel bands of [4]GDA were fluorescently quantified by employing Image J, where the fluorescence intensity of DNA band at 0-h incubation is defined as 1. The assay experiments were conducted as shown in the section SA.1. A small but unnegligible amount of [4]GDA were degraded by DNase I and Exo I. Especially, only about 70% of [4]GDA can be retained after treatment with 10% FBS for 24 h, demonstrating that the resistance of [4]GDA to enzymatic degradation is compromised compared with [2]GDA.

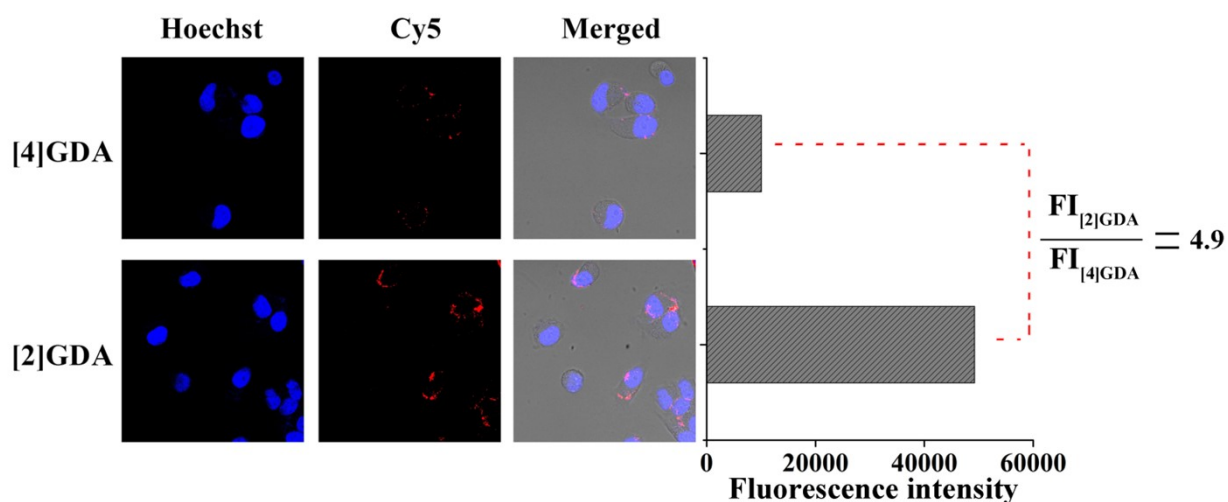


Figure S24. Confocal fluorescence microscopy images of HeLa cells after 2-h incubation with [4]GDA and [2]GDA. [4]GDA and [2]GDA were assembled as described in **Figure S20** and in the Section of “Preparation of catenane-based grid-patterned DNA arrays (GDA)”, respectively. The confocal fluorescence imaging was performed as described in the section **SA.4**. One can notice that the fluorescence intensity of [2]GDA (lower panel) is much higher than [4]GDA (upper panel). The quantitative fluorescence signal indicates about 5-fold higher cell permeability of [2]GDA than [4]GDA.

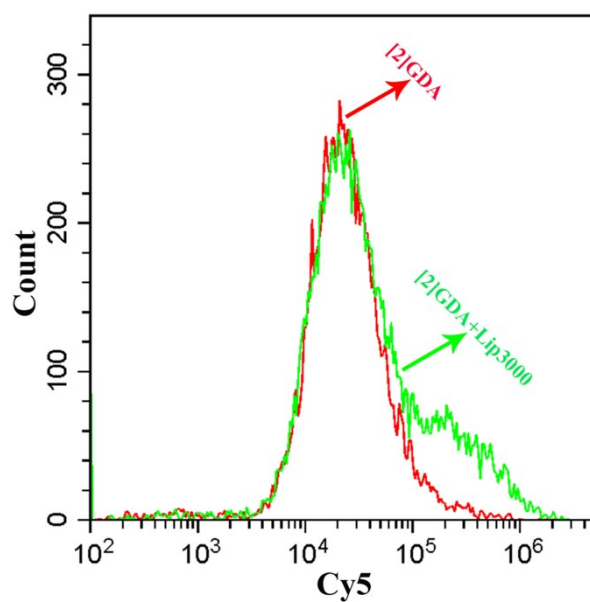


Figure S25. The evaluation of cell permeability of [2]GDA in a comparative manner. The cellular uptake [2]GDA was studied by incubating Cy5-labeled [2]GDA (50 nM) with HeLa cells (1×10^5 cells) for 4 h in the presence (the green line) and absence (the red line) of transfection reagent (Lip3000). The two lines almost coincide well with each other, demonstrating that [2]GDA possesses the outstanding cell permeability comparable to commercial transfection reagent. The experimental details were shown in the section **SA.3**.

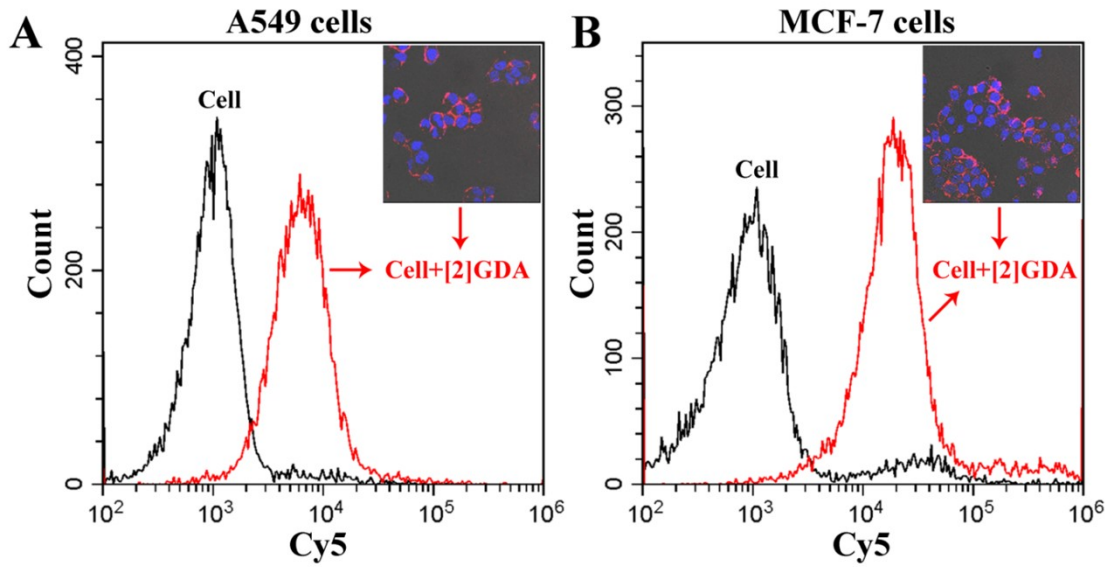


Figure S26. Cellular uptake of [2]GDA-Cy5 (50 nM) by A549 cells (A) and MCF-7 cells (B) after 4-h the incubation. In flow cytometry analysis, the black line indicates blank cells, while the red line means the cells incubated with [2]GDA. The inset is the fluorescence image of the cells after 4-h incubation with [2]GDA. The flow cytometry analysis was carried out as described in the section SA.3, while the confocal fluorescence imaging was performed as described in the section SA.4.

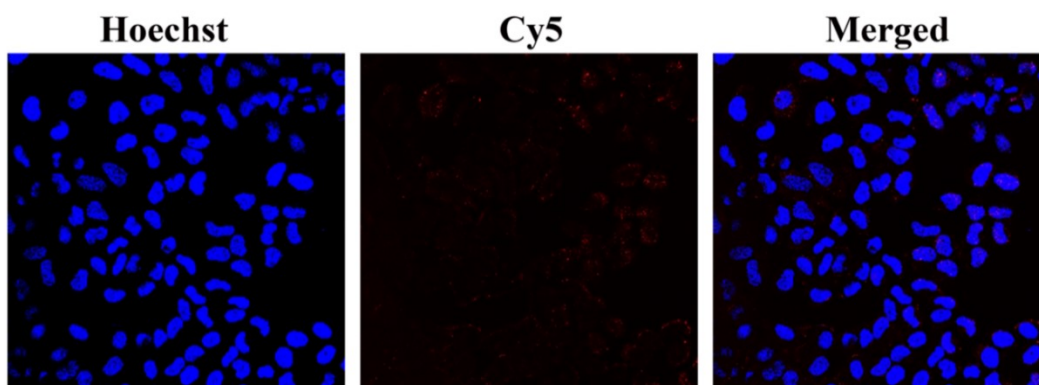


Figure S27. The confocal microscopy images of HeLa cells after 4-h incubation with unannealed PSb-Cy5. The confocal fluorescence imaging was performed as described in the section SA.4. No obvious fluorescence signal is detected, indicating that PSb-Cy5 hardly gets into the cells.

Discussion:

To elucidate the relationship between the structural features of [2]GDA and its outstanding cell permeability, two control studies were conducted. IPSb-Cy5-treated HeLa cells were imaged as the first control, where the expected grid-patterned periodic DNA arrays cannot be assembled owing to the lack of PSa component. **Figure 2B** shows that the fluorescence signal from IPSb-Cy5-treated cells is substantially lower than [2]GDA-Cy5-treated cells even at the same concentration. Moreover, the flow cytometric analysis shows that the fluorescence signal from [2]GDA-Cy5-treated cells is nearly 10 times higher than the signal from IPSb-Cy5-treated cells (**Figure 2C**). As the second control, PSb-Cy5 was directly used to treat the cells without pre-annealing that is required for the formation of longitudinal alignment. As shown in **Figure S27**, no obvious fluorescence signal is detected. These measured data demonstrate that the impressive cell permeability of [2]GDA does originate from the additive effect of palindrome-mediated dual hybridization-based assembly process, the palindromic hybridization-based longitudinal alignment of primary components (PSa or PSb) and canonical base pairing-based perpendicular cross-linking between the secondary building blocks (IPSa and IPSb), showing the structural superiority of two-dimensional catenane monolayer of [2]GDA. Presumably, the two resulting unique structural features can efficiently contribute to the efficient cell entry of [2]GDA: a two-dimensional pattern with large size varying over the micrometer scale and monolayer assembly of double helical structure of DNAs. The former makes the DNA pattern have a surface large enough to increase the interaction probability with the cells and the latter imparts the sufficient flexibility to DNA pattern, thus meeting the requirement of cellular internalization for conformational change. Possible, the endogenous enzymes, for example, DNA topoisomerase, promote the internalization process via uncatenating DNA components.^[S9] Besides, it seems that the ring tension of cross-catenated DNA components might facilitate the cellular uptake.^[S10]

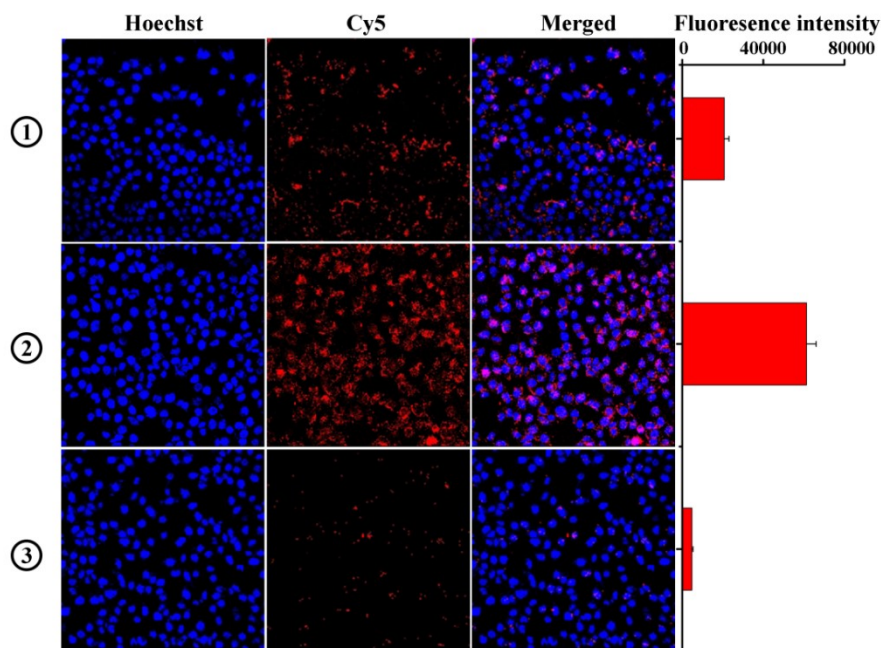


Figure S28. The confocal fluorescence images of HeLa cells treated with [2]GDA of different sizes assembled from different concentrations of PSa and PSb: ① 12.5 μL of 0.8 μM PSa + 12.5 μL of 0.8 μM PSb-Cy5; ② 12.5 μL of 1.6 μM PSa + 12.5 μL of 1.6 μM PSb-Cy5. ③ 12.5 μL of 20 μM PSa + 12.5 μL of 20 μM PSb-Cy5. The experimental processes were described in the section SA.4.

Discussion:

To investigate the relationship between the cell permeability of [2]GDA and its size, the confocal fluorescence imaging was performed after separately incubating HeLa cells with [2]GDA of different sizes for 4 h. For this purpose, besides [2]GDA used throughout the experiments, the smaller and larger ones were explored as the controls. Namely, the hydrodynamic diameter of assembled products in panels ①, ② and ③ are 102 ± 19 nm, 115 ± 11 nm and 940 ± 62 nm, respectively (see the details in **Figure S7** and **S8**). As shown in **Figure S28**, panel ② shows the strongest fluorescence signal compared with panels ① and ③, demonstrating that as-assembled [2]GDA does hold the desirable cellular internalization efficiency. Since the materials of the sizes ranging from 100–500 nm are prone to cell uptake^[S11], the experimental results are reasonable because the size of assembled products in panel ① is close to the minimum value and the objects in panel ③ is much larger than the maximum value.

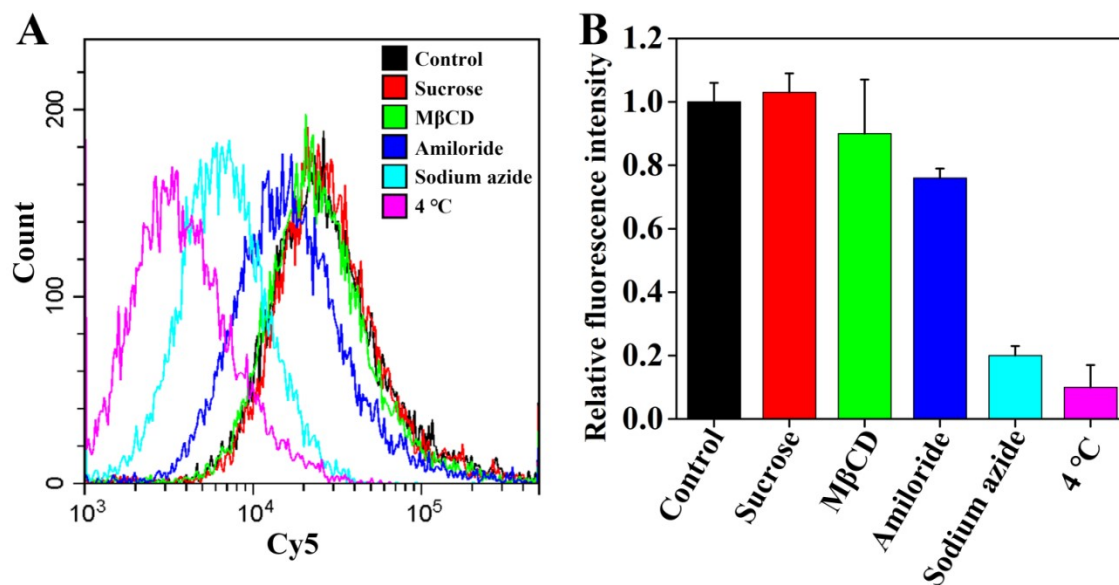


Figure S29. The exploration of endocytosis pathway of [2]GDA-Cy5 using different inhibitors. (A) Flow cytometric analysis of HeLa cells incubated with [2]GDA-Cy5 in the presence of inhibitors. (B) Representative histograms of fluorescence signal from (A). The relative fluorescence intensity of “Control” untreated by inhibitors is defined as 1.

Experimental procedure:

HeLa cells were separately pre-treated with sucrose (an inhibitor for the clathrin-mediated endocytosis, 154 mg/mL), M β CD (an inhibitor for the caveolin-dependent endocytosis, 13 mg/mL), amiloride (an inhibitor for the macropinocytosis pathway, 133 μ g/mL) and sodium azide (an inhibitor for the energy-dependent endocytosis, 1 mg/mL) at 37 °C for 1 h. Subsequently, the culture medium containing specific inhibitor was replaced by fresh DMEM medium in the presence of [2]GDA-Cy5 where the concentration of each DNA component was 50 nM. After incubation for 4 h, the HeLa cells were washed twice with 0.5 mL of SCJ solution, followed by resuspending in 1 mL of SCJ solution. Flow cytometric analysis was performed on a CytoFLEX flow cytometer (Beckman Coulter Biotechnology Co., Ltd, USA). In addition, HeLa cells untreated with the inhibitor were directly incubated with [2]GDA-Cy5 at 4 °C for 4 h to investigate the effect of energy-dependent endocytosis.

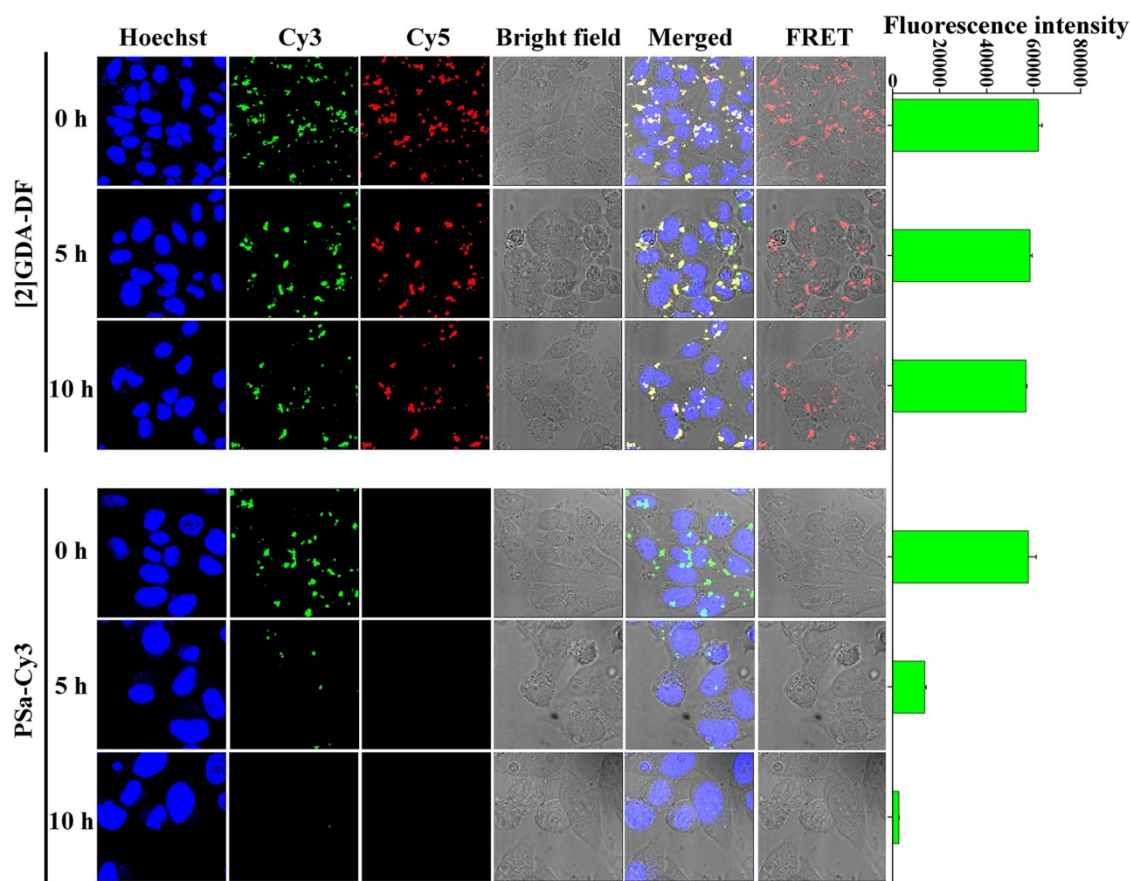


Figure S30. Confocal fluorescence images of [2]GDA-internalized cells. [2]GDA-DF was pre-assembled from PSa-2-Cy3 and PSb-2-Cy5, while PSa-2-Cy3 was used as control. The colocalization assay and FRET efficiency were used to evaluate the intracellular stability of [2]GDA. Blue channel: excitation wavelength of 405 nm, emission wavelength of 450 nm, corresponding to Hoechst 33342 fluorescence; green channel: excitation wavelength of 552 nm, emission wavelength of 565 nm, corresponding to Cy3 fluorescence; red channel: excitation wavelength of 638 nm, emission wavelength of 672 nm, corresponding to Cy5 fluorescence; Merged channel includes the channels of Cy3, Cy5 and bright field; FRET channel: excitation wavelength of 552 nm, emission wavelength of 672 nm. The right panel is the quantitative evaluation of Cy3 fluorescence intensity. The experimental details are described in the section SA.4.

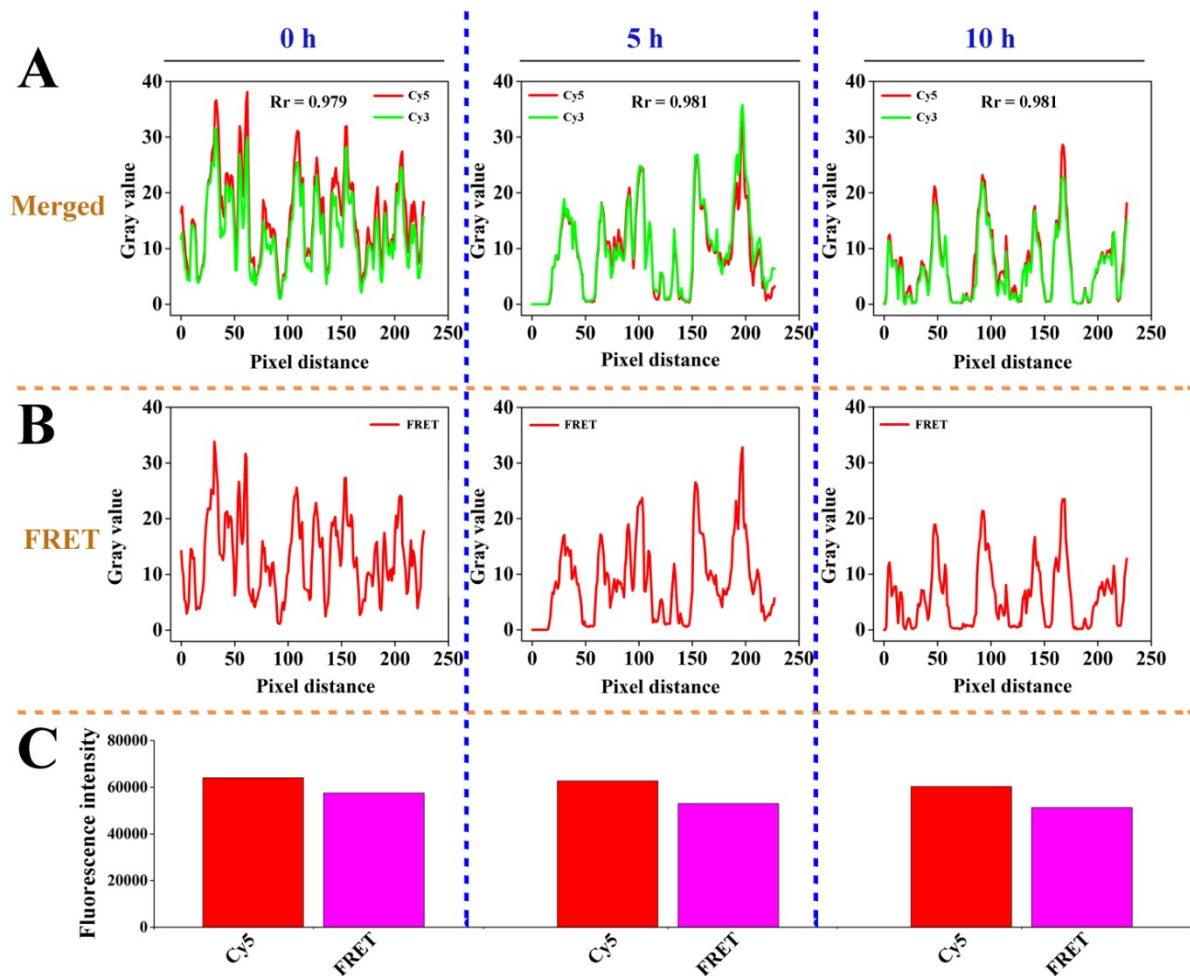


Figure S31. Further evidence for the intracellular stability of [2]GDA obtained from the upper panel of **Figure 30**. (A) The colocalization of Cy3 fluorescence with Cy5 fluorescence obtained from Merged channel; R_r represents the Manders overlap coefficient. (B) FRET signal scanned from the FRET channel; (C) Quantitative evaluation of fluorescence signal from Cy5 channel and FRET channel. These fluorescence analyses were accomplished with Image J.

Discussion:

R_r denotes the Manders overlap coefficient reflecting the degree of colocalization of Cy3 and Cy5. One can be seen that the fluorescence peaks of Cy3 and Cy5 are almost completely overlapped regardless of the incubation time (panel A), and the coefficient value of R_r is more than 0.97 substantially higher than the literature value,^[S12] indicating the structural integrity of [2]GDA subjected to the intracellular degradation. Moreover, the intracellular location of FRET peaks (Panel B) are fully consistent with Cy5 red fluorescence peaks (Panel A), demonstrates the high FRET efficiency. Additionally, as shown in Panel C, no substantial decrease is observed in FRET signal even if incubating for a long time (e.g., 10 h), implying that, during energy transfer from the donor to the acceptor, no substantial energy loss is caused by exposure to extremely complex intracellular environment. If the FRET signal at 0-h incubation is defined as 100%, not less than 90% of fluorescence signal is detected after 10-h incubation. All these measured data confirms the desirable intracellular stability of [2]GDA-DF.

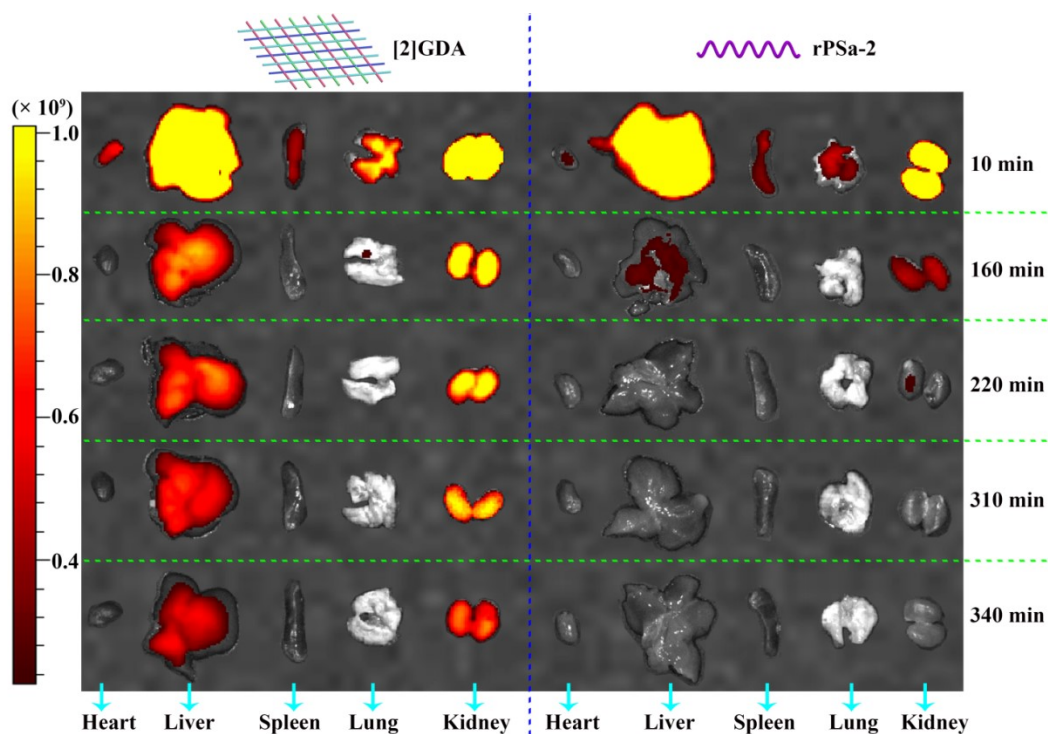


Figure S32. *Ex vivo* organ images of nude mice administered [2]GDA-Cy5 or rPSa-2-Cy5 at specific time intervals. Organs, including heart, liver, spleen, lung and kidney, were fluorescently imaged. There is obvious difference in the fluorescence intensity from liver and kidney between two experimental groups. Specifically, rPSa-2-Cy5 almost was completely degraded in nude mice within 160 min, while [2]GDA-Cy5 can persist over 340 min. The experimental details were shown in the section SA.6.

Discussion:

To further confirm systemic stability of [2]GDA, the dynamic distribution of [2]GDA-Cy5 in major organs (heart, liver, spleen, lung and kidney) of normal nude mice sacrificed at different time intervals was analyzed by *ex vivo* fluorescence imaging where rPSa-2-Cy5 was used as the control. As shown in **Figure S32**, for the five harvested organs, [2]GDA mainly distributes in liver and kidney and fluoresces for a long time post-administration, for example, 340 min, indicating the considerably improved stability superior to the literature DNA materials.^[7b] In contrast, main rPSa-2-Cy5 strands are digested within one hour under identical conditions. To quantitatively evaluate the systemic stability, the total fluorescence intensity of [2]GDA-Cy5 and rPSa-2-Cy5 in the five organs was recorded at 220 min post-administration. This is because rPSa-2-Cy5 is substantially but not completely degraded at this time point. The systemic stability of [2]GDA-Cy5 is estimated to be at least 360 times higher than rPSa-2-Cy5 on the basis of the equation: $(F_a - F_0)/(F_b - F_0)$, where F_a , F_b and F_0 denote the fluorescence intensity of [2]GDA-Cy5, rPSa-2-Cy5 and blank solution, respectively.

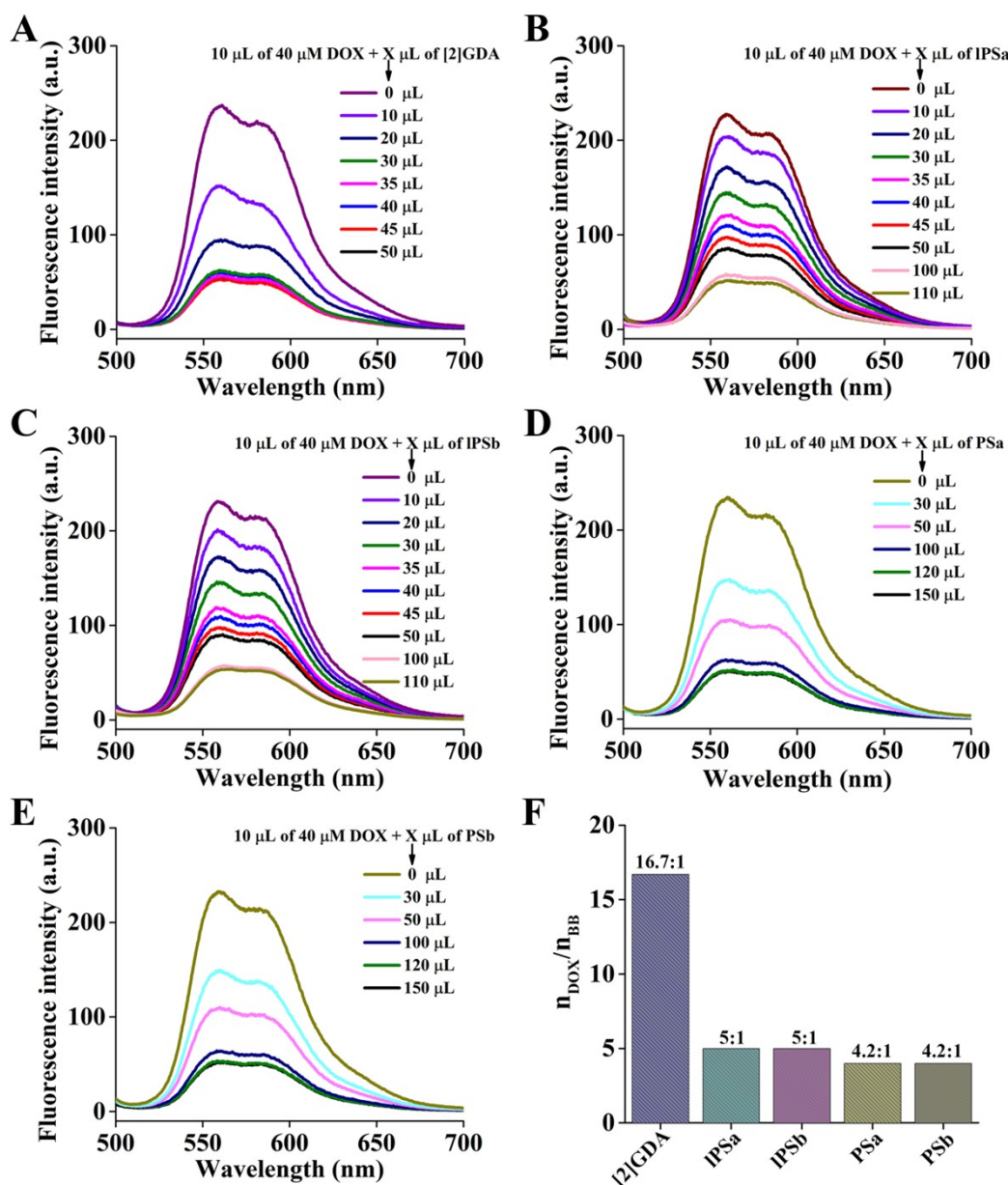


Figure S33. Comparative evaluation of payload capacity of [2]GDA and its counterparts. Fluorescence spectra of DOX in the presence of different DNA assemblies, (A) [2]GDA, (B) IPSa, (C) IPSb, (D) PSa and (E) PSb, each of which contains equal amount of DOX (10 $\mu\text{L} \times 40 \mu\text{M}$). (F) Quantitative data recorded from panels A to E, n_{DOX} and n_{BB} represent the total number ($V \times C$) of DOX and building blocks (BB), respectively, where V is the solution volume and C denotes species concentration. For example, n_{BB} in panel A represents the total number of PSa and PSb, while n_{DOX} is equal to 10 $\mu\text{L} \times 40 \mu\text{M}$. The experimental details were shown in the section SA.2.

Discussion:

As a widely used chemotherapeutic drug, Doxorubicin (DOX) is often used for evaluating DNA-assembly-based delivery vehicles. Dox preferentially intercalates into the π - π stacking of double-stranded G-C base pairs and its fluorescence is quenched via Förster resonance energy transfer (FRET)^[S13]. Thus, using DOX as the drug model, the drug payload capacity of [2]GDA, IPSa, IPSb, PSa and PSb was investigated through the fluorescence measurement. As

shown in **Figure S33A**, DOX fluorescence rapidly decreases with increasing the content of [2]GDA from 0 to 30 μL . Finally, the DOX fluorescence intensity tends to a constant value because of the exhaustion of DOX. Similar fluorescence decay trend is observed in panels **B**, **C**, **D** and **E**. The volumes of [2]GDA, IPSa, IPSb, PSa and PSb used for estimating the payload capability were 30 μL , 100 μL , 100 μL , 120 μL and 120 μL , respectively, at each of which DOXs almost were completely loaded that was confirmed by a fact that no obvious fluorescence decrease is detected even if more DNA building blocks were added. As shown in **Figure S33F**, the quantitative data show that the payload capability of [2]GDA is over three times higher than its counterparts under identical conditions.

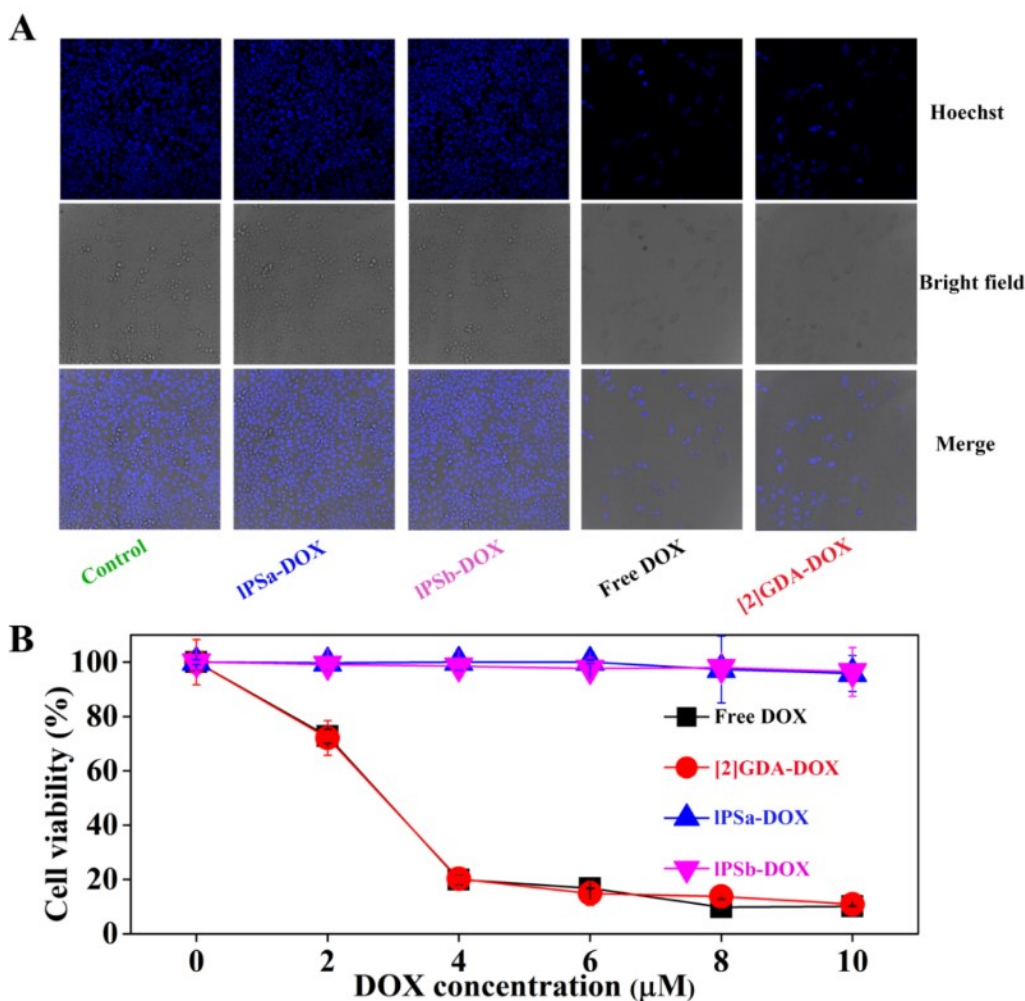


Figure S34. Evaluation of anticancer therapeutic outcome of [2]GDA-DOX at the cellular level. (A) The confocal fluorescence imaging of HeLa cells treated with [2]GDA-DOX, IPSa-DOX and IPSb-DOX at the equivalent concentration of DOX (10 μ M). The intact HeLa cells were used as control. (B) The corresponding MTT assays. The experimental procedures for (A) and (B) are described in the sections SA.4 and SA.5, respectively.

Discussion:

In view of the assembly of [2]GDA directly from IPSa and IPSb, the two semi-finished assemblies were used as the controls. Thus, four DOX-loaded formulations were involved in this section, including [2]GDA-DOX, IPSa-DOX, IPSb-DOX and free DOX. Their therapeutic potency was evaluated by two methods, confocal fluorescence imaging-based cell counting and MTT assay. As shown in **Figure S34A**, compared with the intact cells, the substantial change in cell morphology is observed after treating with [2]GDA-DOX and free DOX, and a dramatic decrease in cell density is detected, demonstrating the desirable therapeutic efficacy of [2]GDA-DOX comparable to the cellular cytotoxicity of equal concentration of DOX. In contrast, IPSa-DOX and IPSb-DOX have no obvious therapeutic response. Moreover, MTT assay shows the consistent results. As shown in **Figure S34B**, the dose-dependent cellular cytotoxicity is observed for HeLa cells treated with [2]GDA-DOX and free DOX, while IPSa-DOX and IPSb-DOX have little toxicity to HeLa cells possibly because of much poorer cell permeability of semi-finished assemblies (seen in **Figure 2B** and **2C**).

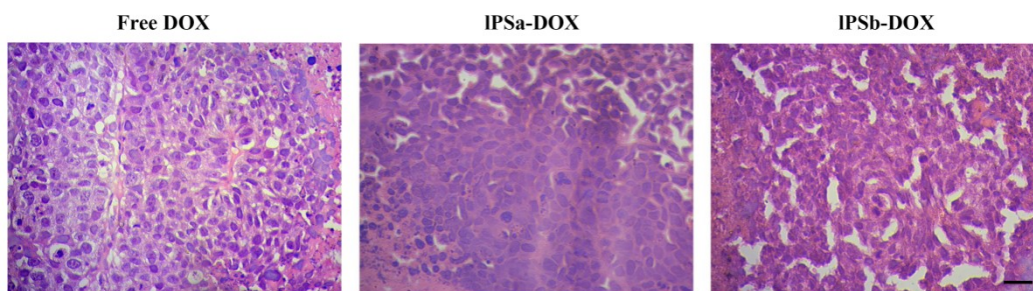


Figure S35. H&E staining of tumor tissues from the nude mice on the 18th day after the first treatment by systemically administrating free DOX, IPSa-DOX or IPSb-DOX (Scale bar, 25 μ m). The experimental details were shown in the section **SA.6**.

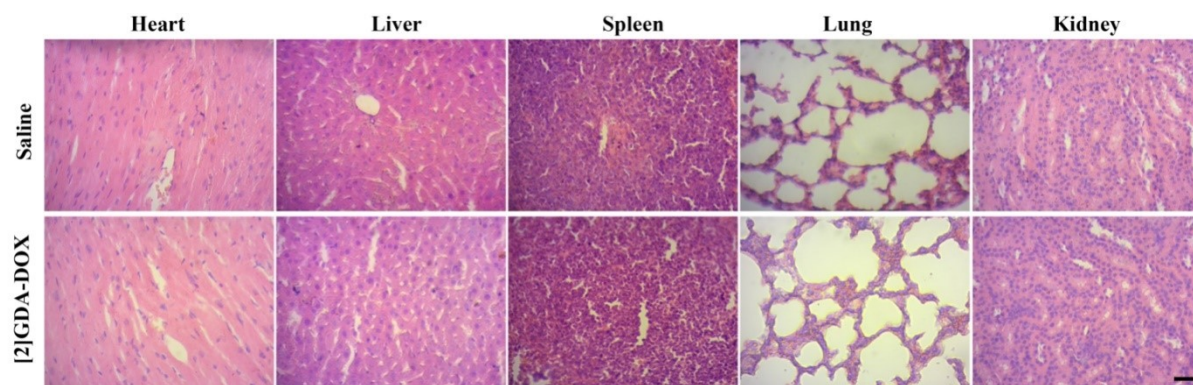


Figure S36. Representative histological analysis of the major organs (heart, liver, spleen, lung and kidney) after H&E staining on the 18th day after the first treatment by systemically administrating [2]GDA-DOX (lower panel) and saline (upper panel) (Scale bar, 25 μ m). The experimental details were shown in the section SA.6.

Discussion:

The histological analysis of different organs, including heart, liver, spleen, lung and kidney, shows that there is no obvious difference between [2]GDA-DOX group and saline group, indicating that no significant damage is found in the organs. These experimental results demonstrate that [2]GDA-DOX has no obvious side effect toward the normal organ tissues even via systemic administration, confirming its potential for targeted cancer therapy.

3. Supporting References

- [S1] C. Wu, S. Cansiz, L. Zhang, I. T. Teng, L. Qiu, J. Li, Y. Liu, C. Zhou, R. Hu, T. Zhang, C. Cui, L. Cui, W. Tan, *J. Am. Chem. Soc.* **2015**, *137*, 4900-4903.
- [S2] Y. Gao, Q. Li, J. Zhang, C. Wu, Z. Shen, C. Xue, H.-T. Chang, Z.-S. Wu, *ACS Appl. Mater. Interfaces* **2020**, *12*, 3341-3353.
- [S3] R. Z. Peng, X. F. Zheng, Y. F. Lyu, L. J. Xu, X. B. Zhang, G. L. Ke, Q. L. Liu, C. J. You, S. Y. Huan, W. H. Tan, *J Am Chem Soc* **2018**, *140*, 9793-9796.
- [S4] Y. Du, P. Peng, T. Li, *Acs Nano* **2019**, *13*, 5778-5784.
- [S5] I. H. Lee, M. K. Yu, I. H. Kim, J. H. Lee, T. G. Park, S. Jon, *J Control Release* **2011**, *155*, 88-95.
- [S6] D. W. Jiang, Y. H. Sun, J. Li, Q. Li, M. Lv, B. Zhu, T. Tian, D. F. Cheng, J. Y. Xia, L. Zhang, L. H. Wang, Q. Huang, J. Y. Shi, C. H. Fan, *Acs Appl Mater Inter* **2016**, *8*, 4378-4384.
- [S7] K. M. Carneiro, G. D. Hamblin, K. D. Hänni, J. Fakhoury, M. K. Nayak, G. Rizis, C. K. McLaughlin, H. S. Bazzi, H. F. Sleiman, *Chem. Sci.* **2012**, *3*, 1980-1986.
- [S8] Z. Wu, H. Wang, M. Guo, L.-J. Tang, R.-Q. Yu, J.-H. Jiang, *Anal. Chem.* **2011**, *83*, 3104-3111.
- [S9] H. Kuai, Z. Zhao, L. Mo, H. Liu, X. Hu, T. Fu, X. Zhang, W. Tan, *J. Am. Chem. Soc.* **2017**, *139*, 9128-9131.
- [S10] a) L. He, D.-Q. Lu, H. Liang, S. Xie, C. Luo, M. Hu, L. Xu, X. Zhang, W. Tan, *ACS Nano* **2017**, *11*, 4060-4066; b) N. Ponnuswamy, M. M. C. Bastings, B. Nathwani, J. H. Ryu, L. Y. T. Chou, M. Vinther, W. A. Li, F. M. Anastassacos, D. J. Mooney, W. M. Shih, *Nat. Commun.* **2017**, *8*, 15654.
- [S11] A. Cherepanova, S. Tamkovich, D. Pyshnyi, M. Kharkova, V. Vlassov, P. Laktionov, *J. Am. Chem. Soc.* **2007**, *325*, 96-103.
- [S12] a) S. Kamberkar, V. S. LeBleu, H. Sugimoto, S. Yang, C. F. Ruivo, S. A. Melo, J. J. Lee, R. Kalluri, *Nature* **2017**, *546*, 498-503; b) A. Lacroix, T. G. W. Edwardson, M. A. Hancock, M. D. Dore, H. F. Sleiman, *J. Am. Chem. Soc.* **2017**, *139*, 7355-7362.
- [S13] a) Y. Burnier, J. Dorier, A. Stasiak, *Nucleic Acids Res.* **2008**, *36*, 4956-4963; b) H. Hiasa, in *DNA Topoisomerases: Methods and Protocols* (Ed.: M. Drolet), Springer New York, New York, NY, **2018**, pp. 47-62.
- [S14] G. Gasparini, G. Sargsyan, E.-K. Bang, N. Sakai, S. Matile, *Angew. Chem. Int. Ed.* **2015**, *54*, 7328-7331.
- [S15] S. J. Lee, M. S. Huh, S. Y. Lee, S. Min, S. Lee, H. Koo, J.-U. Chu, K. E. Lee, H. Jeon, Y. Choi, K. Choi, Y. Byun, S. Y. Jeong, K. Park, K. Kim, I. C. Kwon, *Angew. Chem. Int. Ed.* **2012**, *51*, 7203-7207.
- [S16] X. A. Wu, C. H. J. Choi, C. Zhang, L. Hao, C. A. Mirkin, *J. Am. Chem. Soc.* **2014**, *136*, 7726-7733.
- [S17] C. Xue, S. Zhang, X. Yu, S. Hu, Y. Lu, Z. S. Wu, *Angew. Chem. Int. Ed.* **2020**, *59*, 17540-17547.